



# **Understanding Microscopic Properties of Materials Using Raman Spectroscopy**

**M.Sc. Thesis**

By  
**Kuldeep Barwa**



**Discipline of Physics**  
**INDIAN INSTITUTE OF TECHNOLOGY INDORE**  
**May 2025**





# INDIAN INSTITUTE OF TECHNOLOGY INDORE

## CANDIDATE'S DECLARATION

I hereby certify that the work which is being presented in the thesis entitled **Understanding Microscopic Properties of Materials Using Raman Spectroscopy** in the partial fulfillment of the requirements for the award of the degree of **MASTER OF SCIENCE** and submitted in the **DISCIPLINE OF PHYSICS, Indian Institute of Technology Indore**, is an authentic record of my own work carried out during the time period from December 2024 to May 2025 under the supervision of Professor Rajesh Kumar, Professor, Indian Institute of Technology Indore.

The matter presented in this thesis has not been submitted by me for the award of any other degree of this or any other institute.

*Kuldeep*

Signature of the student with date  
(Kuldeep Barwa)

-----  
This is to certify that the above statement made by the candidate is correct to the best of my/our knowledge.

*Rajesh Kumar*

Signature of the Supervisor of M.Sc. <sup>21/05/2025</sup>  
thesis  
(Professor Rajesh Kumar)

*Dipankar Das*

DPGC, Physics

-----  
**Kuldeep Barwa** has successfully given his M.Sc. Oral Examination held on **14 may 2025**

*Rajesh Kumar*

21/05/2025

Signature of Thesis Supervisor with date  
(Professor Rajesh Kumar)

*Dedicated*  
*to*  
*my Family and Teachers*

# ACKNOWLEDGEMENTS

Without the encouragement of well-wishers, a master's journey that is an emotional rollercoaster of successes is never feasible. As I write this letter to thank everyone who has been with me to support and encourage me along this journey, the two-year adventure has finally come to an end.

First and foremost, my sincerest thanks and gratitude are extended to my guide Professor Rajesh Kumar, for his guidance and motivation to complete this journey. He has been a tremendous mentor for me. His constant support, patience, valuable advice, constructive criticism, and extensive discussion helped me in accomplishing my masters. He has been inculcating inspiration, strength, knowledge, hard work, and confidence as qualities remain source of the light throughout my path of journey.

I express my sincere gratitude to Director IIT Indore, who has been highly encouraging during the entire course of my master's work. I would like to acknowledge all faculty members of the Physics department (IIT Indore) for their kind support and for providing me with experimental facilities. I want to thank the whole physics department which was like a family to me in these two years.

I am indebted to Deb Kumar Rath for his role as both a mentor and a friend. Her insightful advice and encouragement have been a source of motivation at every step of this endeavor.

I was lucky to spend time with my seniors Subin Kaladi Chondath, Love Bansal, Bhumika Sahu, Nikita Ahlawat, Partha S Rout, Shivam Kumar, Sharmistha Singh, Saumya Shrivastava. I would also like to thank all my batchmates and few of my good friends in IIT Indore Prashant Joshi, Arijit Paul, Harshit Dubey, Divyansh Mishra, Kartik Kohli, Faisal Ayub, Pawan Yadav, Mobashshir Mahmood for helping me and giving me joyful moments throughout this journey. I also want to thank my friends from cricket group Sonu Jaiswal, Dikku bhaiya for giving me stress-free and joyful moments. I am deeply grateful to my dear friend from beyond this campus, Jaya Sharma, for her unwavering support and kindness during my challenging times, guiding me through my journey with grace. I would also like to acknowledge Raman facilities by DST-FIST at

IIT Indore. I owe my deepest gratitude to my parents and family for all the sacrifices they made on behalf of me and supported me in all the ups and downs of my life.





# Abstract

This thesis investigates the structural, vibrational, and electronic properties of strontium titanate, a prototypical perovskite, utilizing advanced Raman spectroscopy to elucidate its phase transitions and potential Fano effects, with significant implications for optoelectronic and energy applications. Polarized Raman spectroscopy reveals a cubic-to-tetragonal phase transition at approximately 105 K, characterized by the emergence of first-order  $B_{2g}$  modes at  $144\text{ cm}^{-1}$  and  $445\text{ cm}^{-1}$  at low temperatures (93 K and 88 K), with polarization-dependent intensity variations confirming tetragonal domain alignment and anisotropic vibrational properties, underscoring  $\text{SrTiO}_3$ 's quantum paraelectric behaviour, though local strains indicate areas for further exploration. Additionally, the study explores potential Fano resonance in STO's low-frequency  $\text{TO}_2$ -TA mode, which exhibits asymmetric line shapes suggestive of quantum interference, drawing comparisons with established Fano effects in heavily doped silicon ( $520\text{ cm}^{-1}$  peak) and vanadium pentoxide ( $995\text{ cm}^{-1}$  Ag mode), where temperature-dependent asymmetries and photoexcitation amplify nonlinear behaviours. While anharmonic phonon interactions in  $\text{SrTiO}_3$  hinder definitive Fano confirmation, a framework leveraging silicon and vanadium pentoxide's nonlinear properties is proposed to investigate Fano effects in complex oxides, enhancing understanding of sample's low-temperature dynamics and its potential in oxide electronics. The developed temperature-dependent and polarized Raman methodologies provide a robust approach for studying perovskites, offering valuable insights for optimizing materials in solar cells, microelectronics, and catalysis.

## List of Publications

# List of Figures

<b>Figure 1.1:</b> General structure of perovskites.	<b>19</b>
<b>Figure 1.2:</b> Sir C.V. Raman with the very first setup of the Raman spectrometer (image courtesy, IISc Bangalore).	<b>21</b>
<b>Figure 1.3:</b> Schematic shows the function of the Fano resonance.	<b>23</b>
<b>Figure 1.4:</b> Schematic represents the effect of different perturbations on the Raman spectra.	<b>23</b>
<b>Figure 2.1:</b> General structure of Strontium Titanate.	<b>26</b>
<b>Figure 2.2:</b> Raman spectrum of STO for (a)room temperature and (b) at 93 K.	<b>28</b>
<b>Figure 2.3:</b> (a) Polarization dependent Raman spectra of $\text{SrTiO}_3$ at 93 K from 0 degree to 360 degree showing the first order Raman modes about $144\text{ cm}^{-1}$ and $445\text{ cm}^{-1}$ and (b) Zoomed version of figure a showing the variation of intensity of $\text{B}_{2g}$ mode at $144\text{ cm}^{-1}$ from 0 degree to 360 degree.	<b>29</b>
<b>Figure 2.4:</b> Polar plot of intensity variation of $\text{B}_{2g}$ Raman mode ( $144\text{ cm}^{-1}$ ) as function of polarization angle $\theta$ at 93 K with 633 nm laser.	<b>31</b>
<b>Figure 2.5:</b> Polar plot of intensity variation of $\text{B}_{2g}$ Raman mode ( $144\text{ cm}^{-1}$ ) as function of polarization angle $\theta$ at 88 K with 532 nm laser.	<b>32</b>
<b>Figure 3.1:</b> (a) The temperature dependent Raman spectrum of Strontium Titanate showing the low frequency mode ( $\text{TO}_2\text{-TA}$ ) about $80\text{cm}^{-1}$ and the zoomed version of this mode is plotted (fig b) using 532 nm laser.	<b>38</b>
<b>Figure 3.2:</b> Variation in Raman peak-position with temperature for STO sample and Variation in Linewidth with temperature is plotted.	<b>39</b>

**Figure 3.3** Temperature dependent Raman spectra from heavily doped p type Si using 532 nm laser for the peak at  $520\text{ cm}^{-1}$ . 41

**Figure 3.4:** Variation in the Fano parameter, peak position and line width is plotted respectively as the temperature changes for the peak  $520\text{ cm}^{-1}$ . 42

**Figure 3.5:** Temperature dependent Raman spectrum of  $\text{V}_2\text{O}_5$  material for the peak  $995\text{ cm}^{-1}$  and the zooming version of  $995\text{ cm}^{-1}$  (in the inset). 44

**Figure 3.6:** Variation in the Fano parameter, peak position and line width is plotted respectively as the temperature changes for the peak  $995\text{ cm}^{-1}$ . 45



# Contents

<b>Acknowledgement</b>	<b>6</b>
<b>Abstract</b>	<b>8</b>
<b>List of Publications</b>	<b>9</b>
<b>List of Figures</b>	<b>10</b>
<b>Chapter 1: Introduction</b>	<b>18</b>
<b>Chapter 2: Phase Transition in Strontium Titanate</b>	<b>25</b>
2.1 Why Strontium Titanate:	
2.3 Literature study:	
2.3 Experimental Details:	
2.4 Results and Discussions:	
2.5 Summary:	
<b>Chapter 3: Fano Effect Explored in Different Materials</b>	<b>35</b>
3.1 Nonlinear Phonon behaviour in Heavily Doped Semiconductor Si and $V_2O_5$	
3.2 Temperature-Dependent Raman Spectra of Strontium Titanate:	

3.3 Temperature dependent Raman Spectra of heavily doped Silicon (Si) material:

3.4 Temperature dependent Raman spectrum of  $V_2O_5$  material:

3.5 Summary:

## **Chapter 4: Conclusion**

**49**

## **References**

**51**







# Chapter 1

## Introduction

Perovskites have emerged as a fascinating class of materials in materials science and condensed matter physics, capturing significant attention due to their versatile properties and potential applications in optoelectronic devices. Named after the mineral perovskite ( $\text{CaTiO}_3$ ), these materials share a characteristic crystal structure defined by the general formula  $\text{ABX}_3$ . In this structure, A and B are cations of different sizes, and X is an anion, typically oxygen or a halide. The A cation is usually a larger organic or inorganic ion (e.g., methylammonium, cesium), B is a smaller metal cation (e.g., lead, tin), and X is often a halide (e.g., iodide, bromide) or oxide. This structural flexibility allows perovskites to exhibit a wide range of physical and chemical properties, making them highly tunable for applications such as solar cells, light-emitting diodes (LEDs), photodetectors, and lasers.

Perovskites are particularly notable for their semiconductor properties<sup>1</sup>, which make them promising candidates for next-generation electronic and optoelectronic technologies. A semiconductor is a material with electrical conductivity between that of insulators and conductors, governed by its band gap—the energy difference between the valence and conduction bands. Semiconductors can be intrinsic, where conductivity arises from the material's inherent properties, or extrinsic, where conductivity is enhanced by doping with impurities. The ability to control charge carrier behaviour in semiconductors underpins modern electronics, including transistors, diodes, and photovoltaic devices. Perovskites, as semiconductors, stand out due to their high charge carrier mobility, long carrier diffusion lengths, and tunable band gaps, which can be adjusted by varying the composition of A, B, or X ions.

The optical and electronic properties<sup>2</sup> of perovskites are central to their technological relevance. Optically, perovskites exhibit strong light absorption across a broad spectral range, high photoluminescence quantum yields, and efficient emission, making them ideal for photovoltaic and light-emitting applications. Their band gap can be tailored by substituting halides (e.g., mixing iodide and bromide) or cations, enabling precise control over the wavelengths of light they absorb or emit. Electronically, perovskites possess excellent charge transport properties, with low defect densities and high carrier lifetimes, which enhance the efficiency of devices like solar cells. For instance, lead-halide perovskites have achieved power conversion efficiencies exceeding 25% in solar cells, rivalling traditional silicon-based technologies. Additionally, their ambipolar charge transport—allowing efficient movement of both electrons and holes—further enhances their versatility.

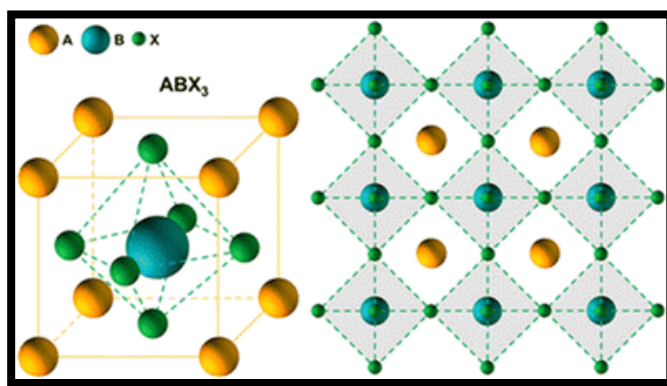


Figure 1.1: General structure of perovskites<sup>3</sup>

Raman spectroscopy serves as a powerful, non-destructive technique for probing the microscopic properties of perovskites, offering detailed insights into their structural and vibrational characteristics. Discovered in 1928 by Sir C.V. Raman and K.S. Krishnan, the Raman effect describes the inelastic scattering of light by matter, where incident photons interact with molecular vibrations or lattice phonons, resulting in a shift in the scattered light's energy. This energy shift, known as the Raman shift, provides a unique fingerprint of the material's vibrational modes, revealing information about its chemical composition, crystal structure, and lattice dynamics. Raman spectroscopy's discovery earned Sir C.V. Raman the Nobel Prize in Physics in 1930, marking a significant milestone in

materials characterization. Unlike other techniques, such as X-ray diffraction (XRD) or infrared (IR) spectroscopy, Raman spectroscopy offers several distinct advantages. It requires minimal sample preparation, is highly sensitive to subtle changes in molecular and lattice structures, and can be performed under ambient conditions without damaging the sample. Compared to IR spectroscopy, which probes dipole moment changes, Raman spectroscopy detects changes in polarizability, providing complementary information about vibrational modes, particularly for symmetric bonds. Raman spectroscopy excels in studying low-frequency lattice vibrations, critical for understanding phase transitions and structural stability in perovskites. Its ability to spatially resolve features at the micrometre scale, especially in confocal Raman setups, further

distinguishes it from techniques like photoluminescence spectroscopy, which primarily focus on electronic transitions. By leveraging Raman spectroscopy, this thesis investigates the microscopic properties of perovskites, including their lattice dynamics, phase behaviour, and molecular interactions, to elucidate the fundamental mechanisms governing their optoelectronic performance. This work aims to advance the understanding of perovskite-based materials for sustainable energy and advanced electronic applications.

Temperature-dependent Raman spectroscopy and polarized<sup>4</sup> Raman spectroscopy further enhance the capability of Raman techniques in studying perovskites. Temperature-dependent Raman spectroscopy involves measuring Raman spectra at varying temperatures to probe the material's response to thermal changes, offering insights into phase transitions, lattice dynamics, and anharmonic interactions. In perovskites, temperature variations can induce structural phase transitions (e.g., from cubic to tetragonal or orthorhombic phases), which alter vibrational modes and are reflected in shifts or broadening of Raman peaks. This technique is particularly valuable for understanding thermal stability and lattice anharmonicity, which influence the optoelectronic performance of perovskites in real-world applications.

Polarized Raman spectroscopy<sup>5</sup> is a specialized technique that enhances the study of vibrational properties in crystalline materials like perovskites by exploiting the polarization of light to probe the symmetry and orientation of vibrational modes. Unlike conventional Raman spectroscopy, which measures the inelastic scattering of light to reveal a material's vibrational fingerprint, polarized Raman spectroscopy controls the polarization of both the incident and scattered light to extract detailed information about the crystal's anisotropic properties. In this method, two primary configurations are used: parallel polarization, where the incident and scattered light polarizations<sup>6</sup> are aligned (e.g., both along the same crystal axis), and cross-polarization, where they are perpendicular (e.g., incident light polarized along one axis and scattered light along an orthogonal axis). The intensity of Raman peaks in these configurations is governed by the Raman tensor, a mathematical representation of how a vibrational mode interacts with polarized light. The Raman tensor, specific to each vibrational mode, depends on the crystal's symmetry and determines which modes are active or suppressed under different polarization conditions. For instance, in a perovskite like  $\text{SrTiO}_3$ , the tensor's components reflect the cubic or tetragonal symmetry, influencing the observed Raman intensities. By



Figure 1.2: Sir C.V. Raman with the very first setup of the Raman spectrometer (image courtesy, IISc Bangalore)

rotating the polarization angle of the incident or scattered light relative to the crystal axes, the intensity of Raman peaks varies, often following a sinusoidal pattern that reveals the mode's symmetry and the crystal's structural orientation.

This intensity variation can be visualized in polar plots, which map the Raman signal as a function of polarization angle, providing a direct way to characterize anisotropic vibrational behaviour. Polarized Raman spectroscopy is particularly powerful for studying phase transitions in perovskites, as changes in crystal symmetry (e.g., from cubic to tetragonal) alter the Raman tensor, leading to distinct intensity patterns in parallel and cross-polarized spectra. This technique thus offers a window into the microscopic lattice dynamics and structural properties critical for understanding the optoelectronic performance of perovskite materials.

In materials like perovskites, which undergo phase transitions with temperature or exhibit strong electron-phonon interactions, these deviations arise because thermal perturbations and phase changes introduce asymmetries in Raman peak shapes. Beyond thermal and confinement effects, phenomena such as doping or electron-phonon coupling, notably the Fano effect, significantly influence Raman spectra. The Fano effect, first described by Ugo Fano in 1961, occurs when a discrete vibrational mode (e.g., a phonon in Raman spectroscopy) interferes with a continuum of electronic states, resulting in asymmetric peak shapes and, in some cases, antiresonance features in the spectra. In perovskites, this electron-phonon interaction is pronounced due to their semiconductor nature, where free carriers interact strongly with lattice vibrations. Unlike thermal effects, which broaden peaks uniformly with rising temperature, doping introduces distinct perturbations by altering carrier concentrations, leading to unique changes in Raman line shapes. Temperature-dependent Raman spectroscopy is crucial for tracking these Fano-induced asymmetries as thermal energy modifies electron-phonon coupling, while polarized Raman spectroscopy, as employed in this study, reveals how these asymmetries depend on crystal orientation and vibrational symmetry. Schematic figures<sup>7</sup> are given below for Fano effect.

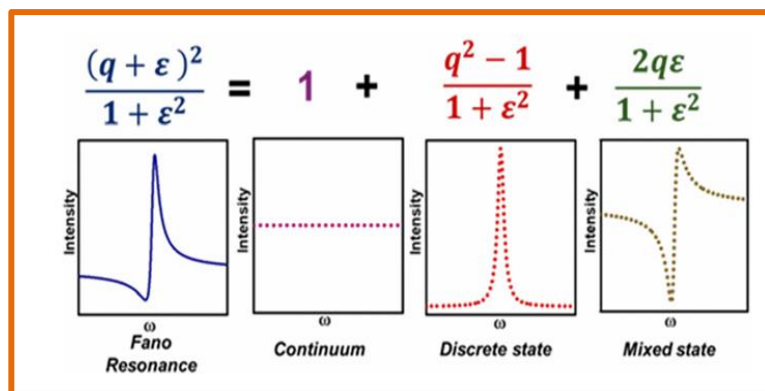


Figure 1.3: Schematic shows the function of the Fano resonance.

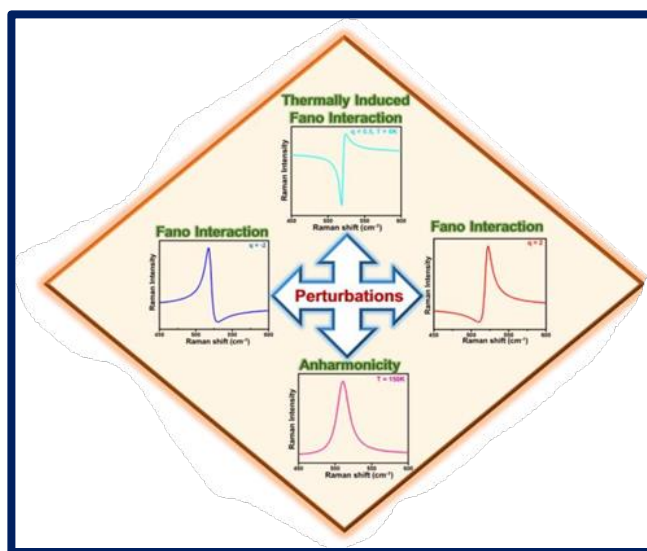


Figure 1.4: Schematic represents<sup>7</sup> the effect of different perturbations on the Raman spectra.





# Chapter 2

## Phase Transition in Strontium Titanate

This chapter investigates the phase transition of single-crystal strontium titanate (STO) using Polarized Raman Spectroscopy. As the material undergoes a phase transition, Raman spectra were collected at room temperature and below 105 K. The sharp peak in the spectra indicates a phase change, and this study explores how the intensity of this peak varies with temperature and angle. Using group theory, the Raman tensor for  $B_{2g}$  mode observed in the Raman spectrum is analysed. The  $B_{2g}$  mode at  $144\text{ cm}^{-1}$  is examined by calculating its intensity at temperatures of 93 K and 88 K, and a polar plot of intensity versus angle was calculated to further characterize the phase transition behaviour.

### 2.1 Why Strontium Titanate:

Single-crystal strontium titanate ( $\text{SrTiO}_3$ ) is a perovskite material known for its highly ordered crystal structure and unique phase transition properties, making it a cornerstone for studying lattice dynamics. STO exhibits quantum paraelectric behaviour, undergoing a structural phase transition at low temperatures (around 105 K) driven by soft phonon modes, without developing full ferroelectric polarization. This transition, sensitive to temperature and strain, highlights its dynamic perovskite characteristics. Decades of research, from foundational studies in the 1960s to recent explorations of its interfaces, have revealed STO's exceptional dielectric properties, superconductivity, and ability to host two-dimensional electron gases. These attributes make STO invaluable for applications such as tunable capacitors, ferroelectric technologies, and oxide electronics. The single-crystal form ensures minimal defects and uniform properties, providing a reliable platform for investigating the fundamental physics and technological potential of perovskites. Raman spectroscopy is an effective method for identifying transitions in these materials. However, in  $\text{SrTiO}_3$ , the emergence of second-order multi-phonon Raman signals complicates the

understanding of the mechanism. Scientists have employed many methodologies and methods to address the confusion linked to Raman effects. It is intriguing to comprehend the process of structural phase transition from cubic to tetragonal through the analysis of Raman spectra.

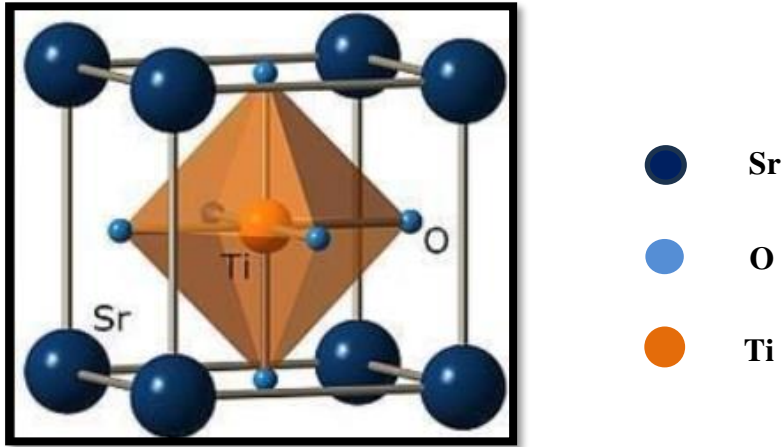


Figure 2.1: General structure of Strontium Titanate<sup>8</sup>

## 2.2 Literature study:

(i) The Raman spectrum of single-crystal SrTiO<sub>3</sub>, as studied by W. G. Nilson<sup>9</sup> et al., reveals key insights into its phase transitions with temperature, down to 25 K. At room temperature, the spectrum is entirely second-order, consistent with the cubic perovskite structure, with phonons near the Brillouin zone boundary, mostly transversely polarized. Upon cooling below the 110 K phase transition, STO exhibits three sharp lines from local modes, not polar transverse-optic (TO) modes, indicating a structural change. This highlights Raman scattering's sensitivity to crystal structure, showing distinct phase transitions in STO. The tetragonal phase of SrTiO<sub>3</sub> likely has a C<sub>4h</sub> point group, as no ferroelectricity or first-order Raman scattering is observed.

(ii) Dodd J. Gray et al.<sup>10</sup>. conducted microscopically resolved polarized Raman spectroscopy on tetragonal SrTiO<sub>3</sub>, focusing on the anisotropic response of first-order Raman peaks within a single tetragonal domain. Their work enabled symmetry assignments to phonons in the first-order Raman spectrum, which is typically obscured by complex, uncontrolled domain structures. By using a translation stage, they mapped

the local domain orientation in a  $3\text{-}\mu\text{m}^3$  crystal volume near the laser focus, comparing these results to wide-field polarized images. This method, leveraging standard instruments, is versatile and applicable to studying related materials, interfaces, and devices.

(iii) A.A. Sirenko et al<sup>11</sup>. conducted the Raman spectrum of  $\text{SrTiO}_3$ , measured at room temperature, reveals patterns linked to second-order scattering, mainly at the Brillouin zone boundary. By examining the energy shifts, researchers determined the single-phonon energies for ten distinct phonon branches used to identify spectral peaks. A new finding is an impurity-related band at  $793\text{ cm}^{-1}$ , observed at 120 K in the tetragonal phase. Impurities in the  $\text{SrTiO}_3$  sample also raised the temperature of the cubic-to-tetragonal phase transition to around 120 K. These energy shifts match well with prior single-crystal studies, confirming the reliability of the results. This echoes Burns and Scott's work on  $\text{PbZr}_x\text{Ti}_{1-x}\text{O}_3$ , which noted that while single crystals offer detailed insights, powder samples can provide much of the same information in some cases.

By taking the references of these literatures and more, the experiment is done on the STO to analyze the intensity variation and confirm the phase change below room temperature from cubic to tetragonal structure.

## 2.3 Experimental Details:

The commercially procured Strontium titanate ( $\text{SrTiO}_3$ ) single crystal (001) has been used for Raman measurement. The Horiba-Jobin Yvon LABRAM-HR spectrometer was used to perform the Raman spectroscopy measurement using excitation wavelengths of 633 nm and 532 nm. Using a 50X long working distance objective and a Linkam stage, the TD Raman measurements were performed at the temperature of 93 K and 88 K. The temperature was held and the sample was manually focused. The spectrometer's integrated software was utilized to adjust the temperature, along with a temperature controller. The polarization dependent measurement has been done by introducing the polarizer in the direction of incident light and an analyzer in the direction of scattered light. The axis of polarization can be rotated by angle 0 to 360

degree by a half wave plate ( $\lambda/2$ ), while the position of the axis of analyzer is fixed. The angle variation is taken the difference of 10 degree. we locally probed the symmetry of one Raman-active ( $B_{2g}$ ) phonon mode. Micro-Raman experiments on  $\text{SrTiO}_3$  require higher excitation powers and longer exposure times compared to materials like graphene due to its 3.2-eV band-gap energy, which is significantly above the 2.33-eV excitation photon energy. That's why the low frequency mode will disappear in 633 nm laser light.

## 2.4 Results and Discussions:

The Raman spectra has been recorded at room temperature and at 93 K at parallel polarization configuration. The Spectrum of  $\text{SrTiO}_3$  at 93 K shows two sharp peaks at about  $144 \text{ cm}^{-1}$  and  $445 \text{ cm}^{-1}$ .

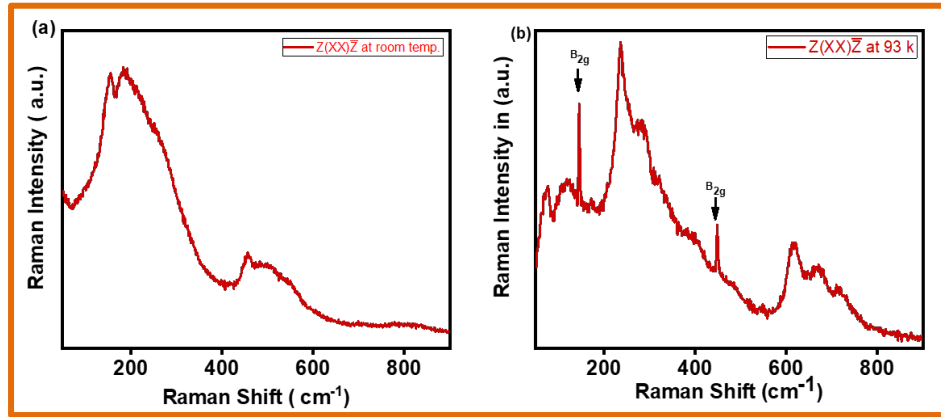


Figure 2.2: Raman spectrum of STO for (a)room temperature and (b) at 93 K

These are the first order Raman modes having symmetry  $B_{2g}$ . These Raman modes can be seen only because of tetragonal phase transition of  $\text{SrTiO}_3$  from cubic phase at low temperature. These Raman modes can be seen only because of tetragonal phase transition of  $\text{SrTiO}_3$  from cubic phase at low temperature. These modes emerge due to the tetragonal phase, which breaks the cubic symmetry and allows first-order scattering. The phase transition is driven by soft phonon modes, particularly the polar transverse-optic modes, which soften (decrease in frequency) as temperature drops,

destabilizing the cubic phase and facilitating the transition to the tetragonal phase. These soft modes play a critical role in the structural rearrangement, enabling the observation of  $B_{2g}$  modes at 93 K, while the second-order scattering at room temperature reflects the harmonic combinations of phonons in the cubic phase.

The Raman mode obeying  $B_{2g}$  symmetry of tetragonal phase are strongly dependent on the polarization of the electric field incident and provides a lot of information about the tetragonality of the crystal structure. So, a polarization dependent Raman measurement has been done at 93 K by rotating the linearly polarized incident light from 0 degree to 360 degree (Figure a and b).

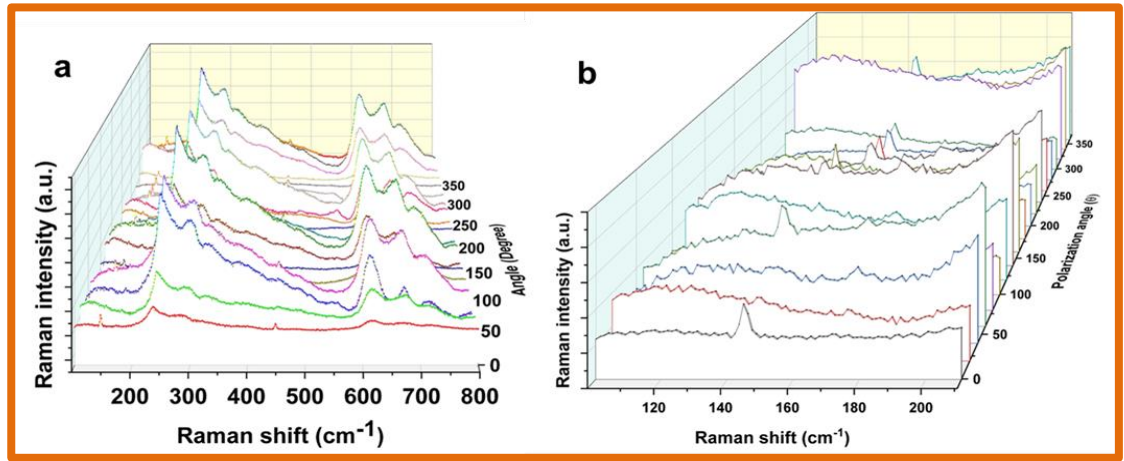





Figure 2.3: (a) Polarization dependent Raman spectra of SrTiO<sub>3</sub> at 93 K from 0 degree to 360 degree showing the first order Raman modes about 144 cm<sup>-1</sup> and 445 cm<sup>-1</sup> and (b) Zoomed version of figure a showing the variation of intensity of  $B_{2g}$  mode at 144 cm<sup>-1</sup> from 0 degree to 360 degree.

To understand the tetragonal phase orientation of SrTiO<sub>3</sub>, the polarization dependent of  $B_{2g}$  Raman mode at 144 cm<sup>-1</sup> has been analyzed as per the mathematical Raman tensor analysis as following way. Since the in transition, the tetragonal axis (c-axis) transition can be happened along any arbitrary direction as the temperature is lowered, it is interesting to investigate the tetragonal domain orientation at a particular temperature and how it changes as the temperature varies.

The phase transition in SrTiO<sub>3</sub> from a cubic to a tetragonal structure, occurring around 110 K, is driven by the softening of an R-point optical phonon, which reduces to zero frequency, lowering the crystal symmetry from the O<sub>h</sub> to the D<sub>4h</sub> point group. This structural change involves elongation of the unit cell along the tetragonal axis, a 45° rotation, and an expansion by a factor of  $\sqrt{2}$  in the basal plane dimensions. At room temperature, the cubic phase restricts Raman scattering to second-order processes due to symmetry selection rules, producing broad spectra from phonon combinations. Upon cooling to 93 K, below the phase transition, the tetragonal phase enables first-order Raman scattering, with distinct B<sub>2g</sub> symmetry modes observed at approximately 144 cm<sup>-1</sup> and 445 cm<sup>-1</sup> in parallel polarization configuration. Additional phonon modes with A<sub>1g</sub>, B<sub>1g</sub>, and E<sub>g</sub> symmetries also become Raman-active in this phase. The intensity of the B<sub>2g</sub> modes varies with the polarization angle  $\theta$  and the orientation of the tetragonal axis (along X, Y, or Z), reflecting the domain structure. The softening of the R-point phonon is critical, as it destabilizes the cubic lattice, facilitating the transition and enabling the emergence of first-order Raman signals characteristic of the tetragonal phase. The relative strength of the Raman response as a function of polarization angle  $\theta$ ,  $I_{ij}(\theta)$ , for B<sub>2g</sub> symmetry and Tetragonal axis domain orientation  $j \in \{X, Y, Z\}$  has been mentioned.

**Table 1: The two-dimensional quasi cubic Raman tensor of B<sub>2g</sub> symmetry in all possible direction of x y and z.<sup>10</sup>**

Raman tensor	$I_x, c  x$	$I_y, c  y$	$I_z, c  z$				
$B_{2g}$ (145 $\text{cm}^{-1}$ , 448 $\text{cm}^{-1}$ )	$\begin{bmatrix} 0 & d & 0 \\ d & 0 & 0 \\ 0 & 0 & 0 \end{bmatrix}$	$\begin{bmatrix} 0 & 0 \\ 0 & d \end{bmatrix}$	$d^2 \sin^4(\theta)$ 	$\begin{bmatrix} d & 0 \\ 0 & 0 \end{bmatrix}$	$d^2 \cos^4(\theta)$ 	$\begin{bmatrix} -d & 0 \\ 0 & d \end{bmatrix}$	$d^2 \cos^2(2\theta)$ 

In a cubic structure, the unit cell parameters are equal, ( $a = b = c$ ) but a change of lattice parameter to ( $a = b \neq c$ ) after a phase transition to a tetragonal structure happened as mentioned earlier. Since the tetragonal axis ( $c$ ) can be elongated in any

arbitrary axis of x, y, or z (if assumed to be aligned in a, b and c axis of unit cell), this can be resolved from the above intensity calculation of polarization tensor (Table 1).

From figure 2.3b the integrated intensity of  $B_{2g}$  Raman mode at  $144\text{ cm}^{-1}$  has been plotted as a function of polarization angle  $\theta$  in polar plot as shown in figure 2.4. It is clear from the plot that it follows the intensity variation  $I_z(\theta)$  as  $d^2\cos^2(2\theta)$ , where d is the Raman tensor element of  $B_{2g}$  symmetry. Since the maximum intensity of the polar plot (figure 2.4) is not exactly at 90, 180 and 270 degrees so the tetragonality changes initiated along the z axis in the domain where laser is focused in the single crystal.

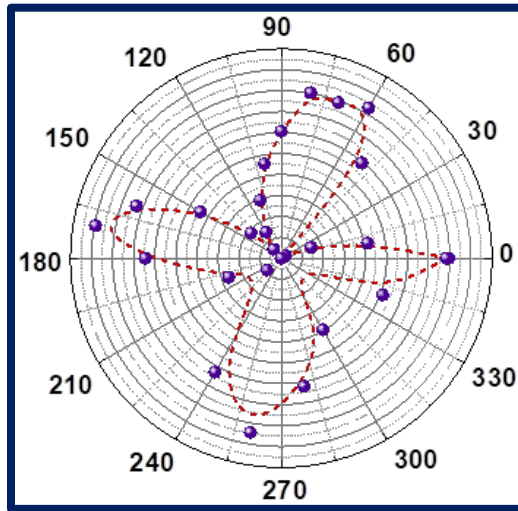


Figure 2.4: Polar plot of intensity variation of  $B_{2g}$  Raman mode ( $144\text{ cm}^{-1}$ ) as function of polarization angle  $\theta$  at 93 K with 633 nm laser.

It will be interesting to investigate the detail transition of tetragonality as the temperature is lowered. STO is a well-known perovskite with a large band gap ( $\sim 3.2\text{ eV}$ ), requiring high-energy excitation like a 532 nm laser ( $\sim 2.33\text{ eV}$ ) to probe its vibrational modes effectively. So, the same experiment is done by cooling the sample by 88 K from a reference temperature for  $B_{2g}$  mode. It can reveal how the tetragonal structure evolves and whether the c-axis undergoes changes in alignment or tetragonality (fig 2.5).

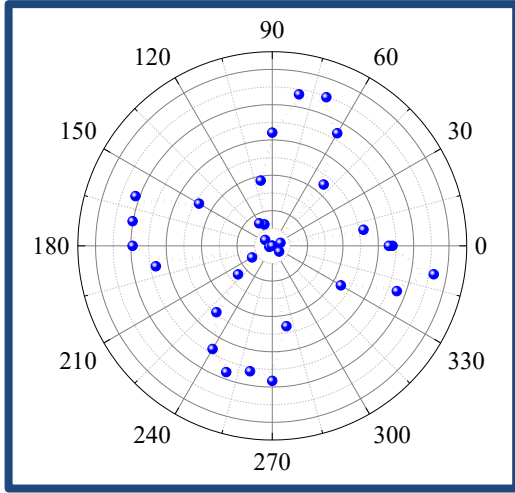


Fig 2.5: Polar plot of intensity variation of B<sub>2g</sub> Raman mode (144 cm<sup>-1</sup>) as function of polarization angle  $\theta$  at 88 K with 532 nm laser.

polar plots for the B<sub>2g</sub> Raman mode at 144 cm<sup>-1</sup> at 93 K (633 nm laser) and 88 K (532 nm laser), suggesting that tetragonality is independent of laser wavelength in this temperature range, though intensity may vary with frequency. STO undergoes a cubic-to-tetragonal phase transition at ~105 K, and at 93 K and 88 K, it is already in the tetragonal phase, characterized by oxygen octahedra rotations. Lowering the temperature further may enhance the tetragonal distortion and stabilize the low-temperature phase.

The angular pattern of the B<sub>2g</sub> Raman mode should stay the same unless a higher-energy laser triggers changes in the crystal's electronic or structural properties. The polar plot's shape depends on the Raman tensor, which reflects the tetragonal symmetry and isn't affected by the laser's frequency. The tetragonal structure and  $c/a$  ratio are determined by the crystal's lattice and temperature, not the laser's wavelength. Therefore, using a higher-frequency laser shouldn't directly change the tetragonality. However, lasers with wavelengths close to the band gap, like 405 nm, might cause minor photoinduced effects that subtly influence the crystal's behaviour.



## 2.5 Summary:

Raman spectroscopy on a SrTiO<sub>3</sub> (001) single crystal revealed first-order B<sub>2g</sub> modes at 144 cm<sup>-1</sup> and 445 cm<sup>-1</sup> at 93 K, confirming a cubic-to-tetragonal transition (~105 K) driven by soft R-point phonons, enabling first-order scattering in the D<sub>4h</sub> symmetry phase. The 144 cm<sup>-1</sup> mode's intensity, varying as d<sup>2</sup>cos<sup>2</sup>(2θ) with polarization angle, indicated z-axis-aligned tetragonal domains. Polar plots at 93 K (633 nm) and 88 K (532 nm) showed consistent tetragonality and increased c/a ratio, but maxima shift from 90°, 180°, and 270° suggested strain or domain misalignment. At lower temperatures, the B<sub>2g</sub> mode in SrTiO<sub>3</sub> shows a stronger intensity, and the polar plot displays sharper peaks, indicating a more pronounced angular dependence. Using a higher-frequency laser boosts the overall intensity further, making these angular patterns even clearer. The tetragonal symmetry of the material remains stable, with the c/a ratio (the ratio of the lattice parameters along the c and a axes) increasing as temperature drops, reflecting a stronger tetragonal distortion. Importantly, the shape of the polar plot stays consistent across different laser frequencies, confirming that the material's tetragonality is not influenced by the laser frequency. This aligns with observations at 93 K and 88 K, where the tetragonal phase was robust.

However, the intensity maxima in the polar plot are not aligned at the expected angles of 90°, 180°, and 270°. This misalignment suggests the presence of local strain, defects, or misaligned domains in the sample, which persist regardless of temperature or laser frequency. Lowering the temperature might reduce these angular shifts if they are caused by thermal vibrations or dynamic disorder, as thermal effects diminish at colder conditions. However, if the shifts persist, it points to structural defects or static strain, possibly tied to the sample's powder nature, as discussed in the prior summary where powder samples yielded results comparable to single crystals. To summarize, the increased B<sub>2g</sub> mode intensity and sharper polar plot maxima at lower temperatures, amplified by higher-frequency lasers, highlight the robust tetragonal symmetry and increased c/a ratio in SrTiO<sub>3</sub>. The consistent polar plot shape across laser frequencies supports the independence of tetragonality from laser effects, while the misaligned

intensity maxima suggest ongoing local strain or defects, potentially linked to impurities or domain issues, which may or may not lessen with further cooling.

# Chapter 3

## Fano Effect Explored in Different Materials

Raman spectroscopy has long been a powerful tool for studying the vibrational properties of materials, but some of its most interesting features appear when we look beyond simple symmetric peaks. The Fano effect, studied in the chapter 1, that distinctive asymmetric line shape that appears in spectra tells that when phonons are interacting with electronic excitations in the material. While this phenomenon has been thoroughly documented in materials like silicon and vanadium pentoxide, its presence in strontium titanate ( $\text{SrTiO}_3$ ) remains less clear, despite the material's interesting properties and technological importance.

What makes this material particularly fascinating is how its properties change with temperature. As the material is cooled, it doesn't undergo a typical ferroelectric transition, but instead enters what we call a quantum paraelectric state. This strange behaviour shows up in its phonon modes too, especially in the famous "soft mode" that becomes unstable at low temperatures. The work focuses on whether these unusual phonons might be interacting with electrons to produce Fano resonances, and how these interactions evolve across different temperature regimes.

In this chapter, the detailed temperature-dependent Raman studies of  $\text{SrTiO}_3$ , tracking how the line shapes change as we vary the temperature from room temperature down to cryogenic ranges. The measurements are designed to catch any signs of Fano interference, particularly in the spectral regions where we expect strong electron-phonon coupling. To help interpret these results, the data will be compared with measurements from silicon and vanadium pentoxide, two materials where Fano effects are well established. The Fano effect manifests distinctly in different material systems. In silicon, the Fano resonance arises from the interaction between optical phonons and free carriers in doped samples, producing characteristic asymmetric line shapes in the first-order Raman spectrum near  $520\text{ cm}^{-1}$ . This phenomenon has been extensively studied since the 1970s, with the Fano parameter  $q$  quantitatively describing the

coupling strength between discrete phonon modes and the electronic continuum. Vanadium pentoxide presents a more complex case, where Fano asymmetries emerge from interactions between lattice vibrations and continuum states associated which is due to photoexcitation which is called resonant Raman scattering and particularly studied in this chapter for the  $995\text{ cm}^{-1}$  region.  $\text{V}_2\text{O}_5$ 's Raman spectra reveal pronounced Fano line shapes that vary with temperature and stoichiometry, reflecting the strong electron-phonon coupling inherent to this transition metal oxide. The motivation behind this work goes beyond just cataloguing another material that shows Fano resonance. Understanding these effects in  $\text{SrTiO}_3$  could give new insights into its peculiar low-temperature behaviour and help explain some of its unusual properties. From a practical perspective, since  $\text{SrTiO}_3$  serves as the foundation for many oxide heterostructures and interfaces, knowing how its phonons interact with electrons could be important for future device applications. This study aims to provide clear evidence for or against Fano resonance in STO, while developing methods that could be applied to other complex oxides.

### **3.1 Nonlinear Phonon behaviour in Heavily Doped**

#### **Semiconductor Si and $\text{V}_2\text{O}_5$ :**

In heavily doped semiconductor  $\text{Si}^{12}$ , an elevated concentration of charge carriers—electrons or holes—triggers significant interactions with the crystal lattice, leading to a proliferation of lattice vibrations, known as phonons, particularly at the boundaries of the material's vibrational zones. These phonons accumulate because their generation outpaces their natural, anharmonic decay, and as temperature increases, this decay becomes nonlinear, intensifying the dynamics. Some phonons form bound states with charge carriers, potentially giving rise to quasiparticles or interference effects, possibly what was referred to as “interferons” in this context. This environment creates fertile ground for the Fano effect, a quantum phenomenon where a discrete energy state interferes with a continuum of states, provided their energies align, producing distinctive asymmetric spectral features detectable through spectroscopic methods. This interference arises from two competing pathways: one linking the ground state to

a specific excited nonlinear form, the Fano effect becomes more complex, driven by strong perturbations, as observed in hybrid systems like metal nanoparticles combined with semiconductor quantum dots. Importantly, no thermodynamic constraints prevent this nonlinear Fano effect from occurring in semiconductors, provided the energy conditions are met and appropriate external stimuli are applied. Given the critical role of semiconductors in technologies such as microelectronics and photovoltaics, investigating this phenomenon is highly compelling. To induce the nonlinear Fano effect, one could apply intense laser pulses to generate excitons or plasmons that couple with phonons, or employ ultrafast laser techniques to capture transient interference states. Strong electric or magnetic fields could modulate the material's energy structure, while elevated temperatures or tailored modifications, such as mechanical strain or precise doping, could align the discrete and continuum energy levels. By leveraging advanced spectroscopy to detect characteristic asymmetric spectral signatures or monitoring time-resolved signals following laser excitation, researchers could probe the presence of the nonlinear Fano effect, potentially unlocking new insights into the behavior of these essential materials.

Transition metal oxides, particularly vanadium pentoxide ( $\text{V}_2\text{O}_5$ ), are widely studied for their unique electronic, structural, and chemical properties, driven by d-electrons and their versatility in catalytic and electrochemical applications.  $\text{V}_2\text{O}_5$ , stable in its  $\text{V}^{+5}$  oxidation state, is theoretically an insulator but exhibits weak vanadyl oxygen bonding, enabling applications in solar cells, antireflection coatings, and electrochromic devices. Its electronic and vibrational properties are well-documented, yet microscopic phenomena like electron-phonon interactions in bulk  $\text{V}_2\text{O}_5$  remain underexplored. The Ag Raman mode of  $\text{V}_2\text{O}_5$  powder displays asymmetry and an antiresonance dip, indicative of electron-phonon interactions, supported by a noticeable electronic Raman background. This mode aligns with the Fano-Raman equation, but laser power and wavelength variations reveal a resonant Fano interaction, weakening at higher laser power, unlike typical Fano systems such as heavily doped silicon. Wavelength-dependent Raman scattering further confirms the resonant nature, highlighting photoexcitation's role when laser energy exceeds the band gap, offering insights into  $\text{V}_2\text{O}_5$ 's vibrational dynamics.

### 3.2 Temperature-Dependent Raman Spectra of Strontium Titanate:

The temperature-dependent Raman spectrum of single-crystal  $\text{SrTiO}_3$  (STO) was obtained using a 532 nm laser. While low-frequency modes were absent in spectra collected with a low frequency laser, these modes, particularly the  $\text{TO}_2\text{-TA}$  mode<sup>13</sup>, were observed with the 532 nm laser. This low-frequency mode exhibits an asymmetric line shape that varies with temperature, suggesting a may be possible Fano effect. The presence of an electronic background and an antiresonance dip further supports this hypothesis. The  $\text{TO}_2\text{-TA}$  mode typically appears in the low-frequency region of STO's Raman spectrum, often below  $\sim 100 \text{ cm}^{-1}$ , depending on experimental conditions. In STO, a perovskite known for its incipient ferroelectricity and quantum paraelectric behaviour, low-frequency modes like  $\text{TO}_2\text{-TA}$  are associated with soft phonons that drive structural phase transitions, such as the cubic-to-tetragonal transition at  $\sim 105 \text{ K}$ .

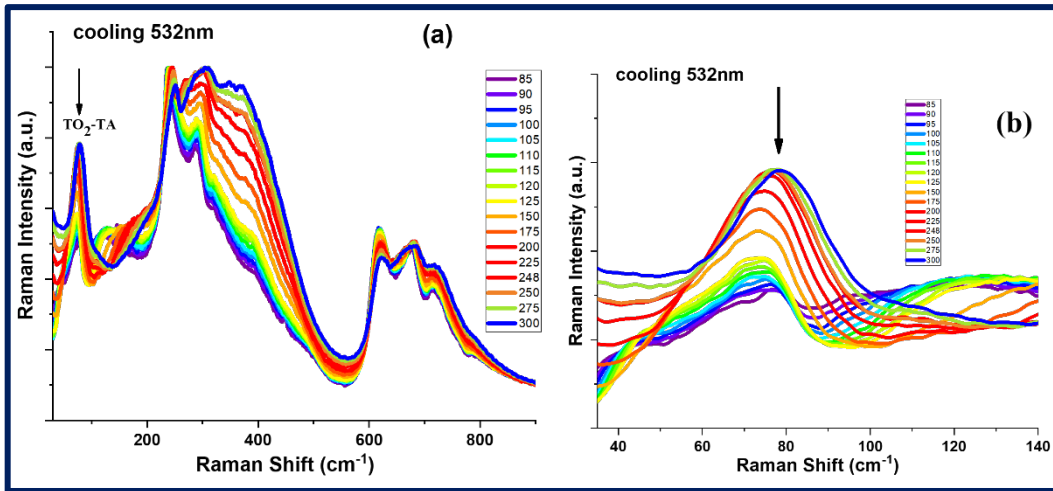


Figure 3.1 (a) The temperature dependent Raman spectrum of Strontium Titanate showing the low frequency mode ( $\text{TO}_2\text{-TA}$ ) about  $80 \text{ cm}^{-1}$  and the zoomed version of this mode is plotted (fig b) using 532 nm laser.

The observed asymmetry in the Raman line shape of the TO<sub>2</sub>-TA mode in single-crystal SrTiO<sub>3</sub>, measured using a 532 nm laser, cannot be immediately attributed to the Fano effect without thorough investigation, as multiple phenomena could contribute to such spectral features. To accurately determine whether the asymmetry arises from a Fano interaction—characterized by interference between a discrete phonon mode and a continuum of electronic states—or from other mechanisms, a detailed analysis of the Raman spectra is essential. Potential alternative phenomena include anharmonic phonon-phonon interactions, disorder-induced broadening, or contributions from overlapping modes, each of which could mimic Fano-like asymmetry. To rigorously confirm the underlying cause, the Raman parameters, specifically the peak position and linewidth of the TO<sub>2</sub>-TA mode, have been fitted as functions of temperature, providing quantitative insights into the mode's behaviour. These parameters are sensitive to changes in lattice dynamics, electron-phonon coupling, and electronic contributions, making them critical for distinguishing between competing mechanisms. For instance, a Fano effect typically manifests as a temperature-dependent asymmetry parameter ( $q$ ) and a characteristic antiresonance dip, accompanied by an electronic background, as observed in the STO spectra<sup>9</sup>. The peak position and line width variance is plotted with the temperature range from 85 K to 300 K in fig (3.2).

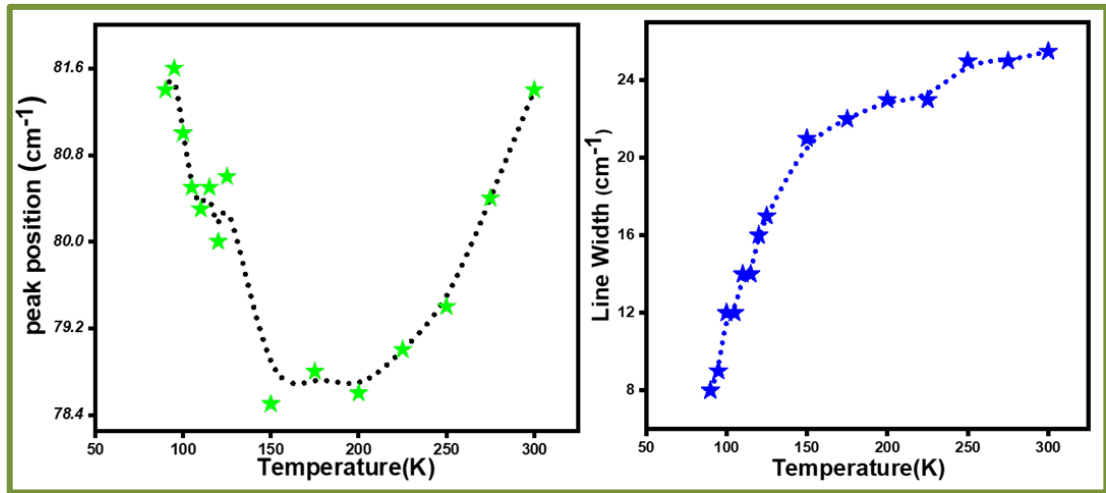


Figure 3.2: Variation in Raman peak-position with temperature for STO sample and Variation in linewidth with temperature is plotted.

By analysing two plots of peak position and line width as functions of temperature, distinct trends in the lattice dynamics of the material emerge. Below 150 K, the peak

position decreases with increasing temperature, indicating a reduction in phonon frequency due to intensified lattice vibrations and anharmonic coupling. Anharmonicity, the deviation from the ideal harmonic oscillator model due to non-linear terms in the potential energy, drives significant phonon interactions. These interactions cause a phonon to decay into two or three lower-energy phonons, conserving energy and momentum, which shortens the phonon lifetime and broadens the spectral line width. Concurrently, the line width increases rapidly, reflecting the decreased phonon lifetime caused by enhanced phonon decay processes. This behaviour confirms that anharmonicity dominates up to 150 K, with increased thermal energy amplifying vibrational interactions and reducing phonon frequencies. Beyond 150 K, the peak position reverses and increases with temperature, exhibiting non-linear behaviour, while the line width stabilizes, suggesting that anharmonic phonon decay is no longer the primary mechanism.

At higher temperatures, other phenomena, such as thermal expansion, electronic interactions, or higher-order scattering processes, likely become dominant, counteracting the frequency reduction and limiting further spectral broadening. There is also another statement can be said that above 150 K, in the cubic phase, the material exhibits semiconductor-like behaviour with increased charge carriers, causing the peak position to rise due to electron-phonon coupling and the line width to stabilize as scattering saturates. This transition highlights the shift from lattice-driven dynamics to charge carrier-mediated vibrational properties.

- The temperature-dependent plots of peak position and line width in strontium titanate ( $\text{SrTiO}_3$ ) show non-linear behaviour, potentially exhibiting asymmetric line shapes suggestive of the Fano effect, but it remains uncertain whether this is due to Fano resonance or other phenomena. We examined well-established publications on the Fano effect in various materials, which reveal similar non-linear trends in peak position and line width, often accompanied by asymmetric spectral features. By analyzing these materials, we seek to determine whether the observed phenomena in  $\text{SrTiO}_3$  stated from Fano resonance or other underlying mechanisms.



### 3.3 Temperature dependent Raman Spectra of heavily doped Silicon (Si) material:

A TD Raman spectroscopy have been carried out from heavily doped p-type Si<sup>14</sup> material using 532 nm laser for 520 cm<sup>-1</sup> peak to investigate the thermal response of phonons through possible phonon-phonon and electron-phonon interactions in sample.

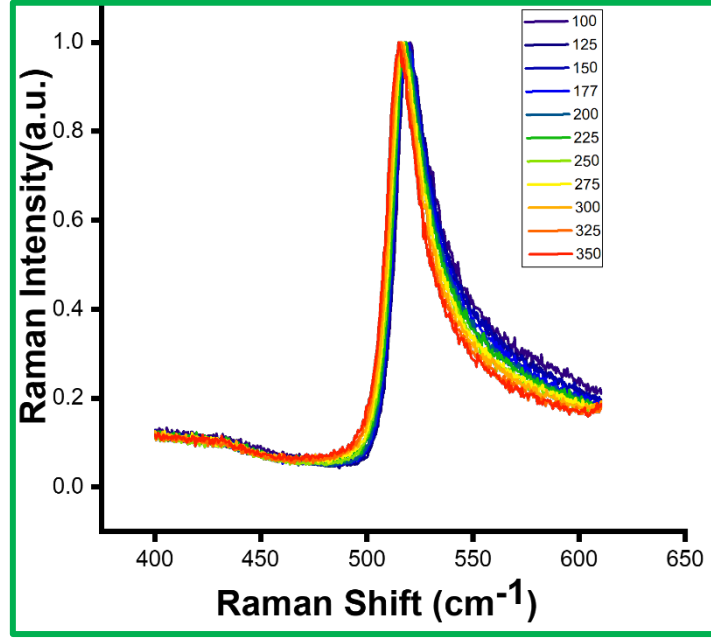


Figure 3.3 Temperature dependent Raman spectra from heavily doped p type Si using 532 nm laser for the peak at 520 cm<sup>-1</sup>.

Heavy acceptor doping significantly influences the position and width of one-phonon Raman lines in silicon (Si), as described previously. In Si, this doping leads to a "softening" of the crystal due to carrier redistribution, which shifts the phonon frequency toward lower energies in the Raman spectrum. Building on this, the temperature-dependent Raman spectrum of heavily doped Si, as shown in Figure 3.3, reveals additional complexities. As the temperature decreases, an asymmetric line shape emerges, characterized by an anti-resonance dip on the low-energy side and asymmetry on the high-energy side. This asymmetry<sup>15</sup> is supported by the Raman electron background, which indicates Fano resonance for the peak. The Fano resonance arises from the interference between the discrete phonon state and the

continuum of electronic states, further modulated by the doping-induced changes in the band structure. These observations connect directly, where doping alters the valence band and carrier dynamics, contributing to the observed spectral features and reinforcing the impact of electronic effects on the phonon behaviour in heavily doped Si.

To analyse more, how the Fano effect does vary with temperature the Raman parameter the peak position, line width and fano parameter are fitted in fig 3.4.

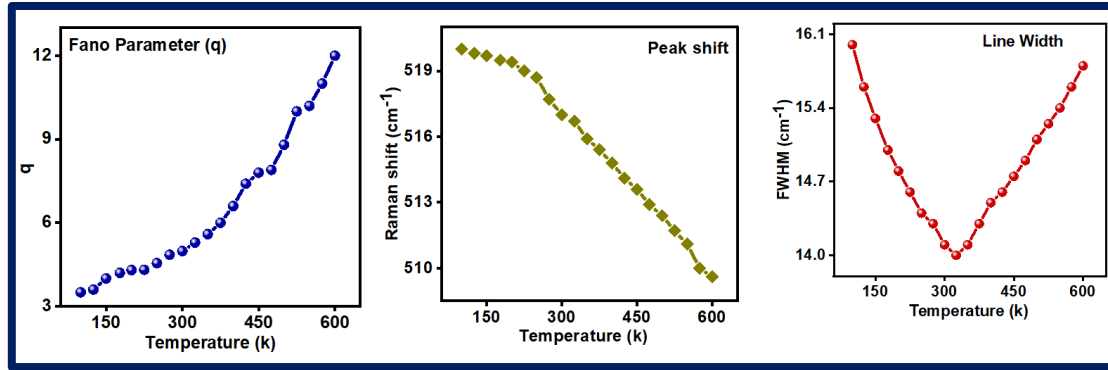


Figure 3.4: Variation in the Fano parameter, peak position and line width is plotted respectively as the temperature changes for the peak 520 cm<sup>-1</sup>.

As temperature increases, a red shift in the Raman peak position of heavily doped silicon (Si) is observed, attributed to Fano interaction, as described in Balkanski theory. This interaction arises from the quantum interference between the discrete optical phonon mode and the continuum of electronic states induced by heavy doping, as discussed earlier. The red shift reflects a decrease in phonon frequency, consistent with the “softening” of the crystal due to doping-induced carrier redistribution and valence band splitting, which lowers the crystal’s free energy. Additionally, anharmonic effects contribute to this behaviour, as evidenced by the peak shift and the reduction in line intensity with increasing temperature. Anharmonicity, stemming from nonlinear interactions between phonons, leads to thermal expansion and phonon-phonon scattering, further softening the lattice and reducing the phonon lifetime.

However, the Raman line width exhibits nonlinear behaviour with temperature. Below and up to room temperature (~300 K), the line width decreases, indicating that electron-phonon interactions dominate. These interactions, enhanced by the high

carrier concentration from heavy doping, couple the phonon to the electronic continuum, broadening the line at lower temperatures where carriers are less thermally scattered. Above room temperature, the line width increases, suggesting that anharmonic phonon-phonon interactions become dominant. This increase is driven by enhanced lattice vibrations due to thermal perturbations, which amplify phonon scattering and reduce phonon coherence.

The Fano parameter, which quantifies the strength of the Fano resonance, increases with temperature, indicating a weakening of the Fano effect. This trend occurs because, above room temperature, anharmonic interactions overshadow the Fano interference. Thermal agitation enhances lattice vibrations, increasing the asymmetry in the Raman line shape, as observed in the temperature-dependent spectrum (Figure 3.3). This asymmetry, with an anti-resonance dip on the low-energy side and broadening on the high-energy side, aligns with the doping-induced electronic modifications discussed previously. The interplay between anharmonicity and electron-phonon coupling thus governs the Raman spectral features, with anharmonicity prevailing at higher temperatures due to increased thermal energy disrupting the delicate balance of Fano interference.

### **3.4 Temperature dependent Raman spectrum of $V_2O_5$ material:**

As the previously discussed for the Silicon material the temperature dependent Raman spectrum is observed (fig 3.5) for polycrystalline  $V_2O_5$  material also using 532 nm laser light for the peak  $995\text{ cm}^{-1}$  where the Fano effect is well established in this material.

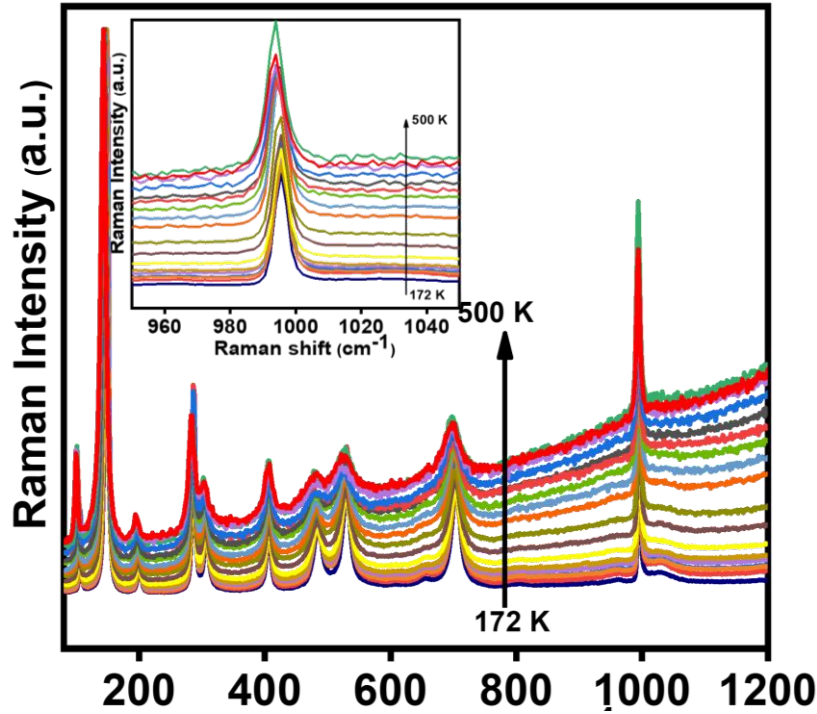


Figure 3.5: Temperature dependent Raman spectrum of  $V_2O_5$  material for the peak  $995\text{ cm}^{-1}$  and the zooming version of  $995\text{ cm}^{-1}$  (in the inset)

The temperature-dependent Raman spectrum of vanadium pentoxide ( $V_2O_5$ ) exhibits an asymmetric line shape, indicative of a Fano effect<sup>16</sup> at the  $995\text{ cm}^{-1}$  peak, associated with the  $A_g$  vibrational mode. This mode originates from the z-axis oscillation of terminal oxygen atoms, a characteristic signature of  $V_2O_5$ . The Fano effect manifests as an asymmetric spectral profile with an anti-resonance dip on the low-energy side, resulting from quantum interference between the discrete phonon<sup>17</sup> mode and a continuum of electronic states induced by photoexcitation. Excitation at  $532\text{ nm}$ , aligning with  $V_2O_5$ 's optical band gap of approximately  $2.3\text{ eV}$ , enhances resonant Raman scattering, generating charge carriers that amplify the Fano interaction. Analogous to the carrier-induced band structure modifications in heavily doped silicon, the photoexcited carriers in  $V_2O_5$  modulate phonon properties through electron-phonon coupling.

To investigate how the asymmetry Raman line shape is varying the temperature. The peak position, line width and Fano parameter are fitted with the temperature variations in fig 3.6.

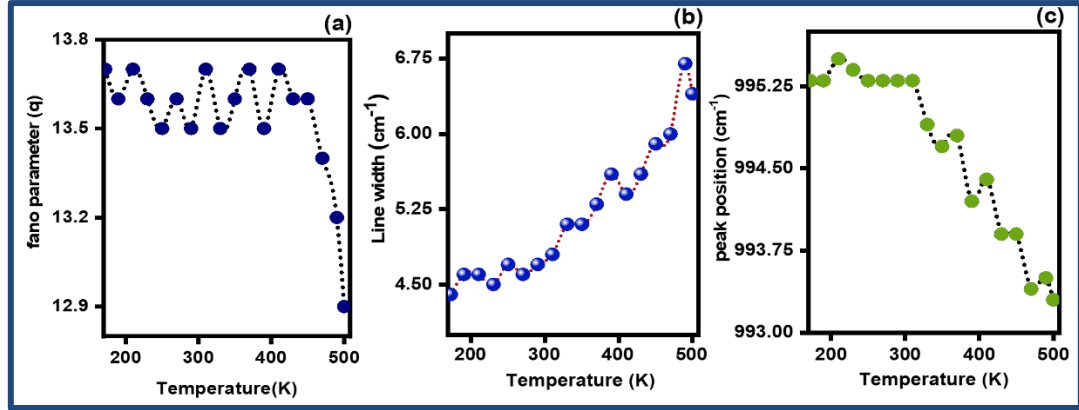


Figure 3.6 Variation in the Fano parameter, peak position and line width is plotted respectively as the temperature changes for the peak 995 cm<sup>-1</sup>.

In the case of V<sub>2</sub>O<sub>5</sub>, the optical band gap energy plays a crucial role in determining the resonance condition for Raman scattering. When the excitation wavelength aligns with the material's band gap energy, it enhances the resonant Raman scattering process, leading to intensified phonon-electron interactions. This resonant condition significantly impacts the Fano parameter, as the coupling between discrete phonon modes and the continuum of electronic states becomes stronger, increasing asymmetry in the Raman line shape. The oscillatory behaviour of the Fano parameter at lower temperatures suggests that interference effects are present but remain relatively stable, likely due to minimal fluctuations in electronic density. However, above 300 K, the rapid enhancement of the Fano strength indicates an increase in electronic interactions, potentially driven by higher thermal energy enabling more effective coupling between charge carriers and vibrational states. For linewidth broadening and peak position shifts, charge carrier dynamics and anharmonic interactions emerge as key factors. As temperature rises, carrier density<sup>18</sup> may increase, altering electron-phonon interactions and contributing to spectral modifications. Anharmonicity, arising from phonon-phonon scattering, becomes more pronounced at elevated temperatures, leading to further broadening of the Raman peaks. While phonon-phonon coupling plays a role in linewidth expansion, the charge carrier dynamics dictate peak position shifts by

modifying vibrational frequencies. The observed stability up to 300 K suggests a regime dominated by weaker phonon interactions, whereas beyond this temperature, stronger electron-phonon and anharmonic contributions drive more pronounced changes. Thus, understanding these effects allows a deeper insight into the thermal and electronic behaviour of the material, linking Raman spectral variations directly to fundamental physics concepts governing phonon and charge carrier interactions.

Beyond the 300 K threshold, pronounced changes emerge, marking a shift in the underlying scattering mechanisms. The rapid enhancement of the Fano strength, the accelerated broadening of the linewidth, and the continued decrease in peak position collectively indicate the growing influence of anharmonic interactions. At elevated temperatures, the phonon-electron coupling intensifies, amplifying the Fano effect, which becomes more dominant than anharmonicity in governing the spectral characteristics. This suggests that, as temperature increases, electronic states experience enhanced mobility or increased density, thereby strengthening their interactions with phonons. The presence of a subtle phase transition or an alteration in the electronic structure around 300 K could lead to a higher availability of continuum states, further reinforcing the Fano resonance.

These findings highlight the complexity of temperature-dependent Raman behaviour, where multiple competing effects shape the spectral response. The delicate interplay between phonon scattering, electronic interactions, and anharmonic contributions underscores the importance of detailed spectral analysis to decipher the relative contributions of each factor. The observed trends suggest that while phonon-phonon anharmonicity plays a role, it is the evolving nature of electronic states and their interaction with discrete vibrational modes that primarily govern the Raman response above 300 K. This insight provides valuable information about the underlying material properties, aiding in the interpretation of Raman spectral variations as a function of temperature. Understanding these phenomena not only contributes to fundamental condensed matter physics but also has implications for materials engineering, where controlling phonon-electron interactions can lead to the optimization of thermal and electronic properties in advanced materials systems.

### 3.5 Summary:

This chapter investigates the temperature-dependent Raman spectroscopy of heavily doped silicon (Si), vanadium pentoxide ( $\text{V}_2\text{O}_5$ ), and strontium titanate ( $\text{SrTiO}_3$ ), focusing on the interplay of phonon dynamics, electron-phonon interactions, and the Fano effect. Each material exhibits unique spectral features influenced by temperature, doping, and electronic structure, providing insights into their vibrational and electronic properties critical for applications in microelectronics, photovoltaics, and catalysis.

In heavily doped p-type silicon, the Raman spectrum of the  $520\text{ cm}^{-1}$  peak reveals a temperature-dependent Fano resonance, characterized by an asymmetric line shape with an anti-resonance dip. As temperature increases, the peak position redshifts due to lattice softening from doping-induced carrier redistribution and anharmonic phonon-phonon interactions. The linewidth decreases up to 300 K, driven by dominant electron-phonon coupling, but increases above this temperature as anharmonic effects prevail. The Fano parameter weakens with rising temperature, indicating that thermal agitation enhances anharmonicity, overshadowing Fano interference.

For polycrystalline  $\text{V}_2\text{O}_5$ , the  $995\text{ cm}^{-1}$   $A_g$  mode displays a Fano effect, marked by an asymmetric line shape due to interference between the phonon mode and photoexcited electronic states. Below 300 K, the peak position<sup>19</sup> and linewidth remain stable, with resonant Raman scattering dominating and the Fano parameter showing oscillatory but constant behaviour. Above 300 K, the Fano strength increases, the linewidth broadens rapidly, and the peak position decreases, suggesting a transition from resonant scattering to a regime where the Fano effect overshadows anharmonic interactions, possibly due to enhanced electron-phonon coupling or a subtle electronic transition.

The confirmed Fano resonance in Si and  $\text{V}_2\text{O}_5$ , characterized by temperature-dependent Fano parameter variations and asymmetric line shapes, provides a robust reference for interpreting  $\text{SrTiO}_3$ 's spectra. However, further analysis, such as fitting the Fano parameter or conducting wavelength-dependent Raman studies, is necessary to definitively confirm Fano interference in  $\text{SrTiO}_3$ . These comparative findings highlight the complex interplay of lattice dynamics, electron-phonon coupling, and quantum interference across these materials, offering valuable insights into the

vibrational properties of  $\text{SrTiO}_3$  and its potential Fano-related behaviour, with implications for its use in ferroelectric and electronic applications.



# Chapter 4

## Conclusion:

This thesis has delved into the fascinating world of perovskites, with a particular focus on strontium titanate, to uncover the intricate interplay of their structural, vibrational, and electronic properties using advanced Raman spectroscopy techniques. By exploring the phase transitions and potential Fano effects in  $\text{SrTiO}_3$ , alongside comparative studies with heavily doped silicon (Si) and vanadium pentoxide ( $\text{V}_2\text{O}_5$ ), this work has contributed to a deeper understanding of these materials' behaviors, which are pivotal for next-generation optoelectronic and energy applications. The journey through this research has been both challenging and rewarding, revealing the power of spectroscopy to probe the microscopic dynamics that govern material performance.

**Chapter 2** illuminated the cubic-to-tetragonal phase transition in  $\text{SrTiO}_3$ , observed around 105 K, through polarized Raman spectroscopy. The emergence of first-order  $B_{2g}$  Raman modes at  $144\text{ cm}^{-1}$  and  $445\text{ cm}^{-1}$  at low temperatures (93 K and 88 K) confirmed the structural shift driven by soft phonon modes. The polarization-dependent intensity variations, mapped through polar plots, revealed the alignment of tetragonal domains and the material's anisotropic vibrational properties. These findings underscore  $\text{SrTiO}_3$ 's unique quantum paraelectric behavior and its sensitivity to temperature, making it a model system for studying lattice dynamics in perovskites. The consistent tetragonal symmetry across different laser wavelengths (633 nm and 532 nm) and the increasing  $c/a$  ratio at lower temperatures highlight the robustness of the phase transition, though slight misalignments in intensity maxima suggest local strains or defects that warrant further exploration.

Chapter 3 expanded the investigation to explore the potential Fano effect, a quantum interference phenomenon, in  $\text{SrTiO}_3$ , drawing comparisons with well-established Fano resonance behaviours in heavily doped Si and  $\text{V}_2\text{O}_5$ <sup>20</sup>. In heavily doped Si, the  $520\text{ cm}^{-1}$  peak exhibits clear Fano resonance, with temperature-dependent asymmetries driven by electron-phonon coupling and anharmonic interactions, as documented in prior studies. Similarly,  $\text{V}_2\text{O}_5$ 's  $995\text{ cm}^{-1}$  Ag mode shows pronounced Fano

characteristics, amplified by photoexcitation and resonant Raman scattering, particularly above 300 K, consistent with established research. In  $\text{SrTiO}_3$ , the low-frequency  $\text{TO}_2$ -TA mode displays asymmetric line shapes that suggest possible Fano interference, but definitive confirmation remains elusive due to competing mechanisms, such as anharmonic phonon interactions. By leveraging the known nonlinear behaviours of Si and  $\text{V}_2\text{O}_5$  as a reference<sup>21</sup>, this study proposes a framework for investigating potential Fano effects in complex oxides like  $\text{SrTiO}_3$ , providing insights into its enigmatic low-temperature behaviour and its prospects in oxide electronics.

The significance of this work lies not only in its scientific contributions but also in its implications for real-world applications. Perovskites like  $\text{SrTiO}_3$  are at the forefront of sustainable energy technologies, from high-efficiency solar cells to tunable electronic devices. Understanding their phase transitions and electron-phonon interactions is crucial for optimizing their performance in harsh conditions, such as varying temperatures. The methodologies developed here, particularly the use of temperature-dependent and polarized Raman spectroscopy, provide a blueprint for studying other perovskite materials, paving the way for innovations in microelectronics, photovoltaics, and catalysis.

## REFERENCES

1. Assirey, E. A. R. Perovskite synthesis, properties and their related biochemical and industrial application. *Saudi Pharmaceutical Journal* **27**, 817–829 (2019).
2. Magnetic, Electronic, and Optical Properties of Perovskite Materials | SpringerLink.  
[https://link.springer.com/chapter/10.1007/978-981-15-1267-4\\_2](https://link.springer.com/chapter/10.1007/978-981-15-1267-4_2).
3. Figure 1. Schematic illustration of the perovskite crystal structure... *ResearchGate*  
[https://www.researchgate.net/figure/Schematic-illustration-of-the-perovskite-crystal-structure-where-A-and-B-are-cations-and\\_fig1\\_361880950](https://www.researchgate.net/figure/Schematic-illustration-of-the-perovskite-crystal-structure-where-A-and-B-are-cations-and_fig1_361880950).
4. Saito, R., Tatsumi, Y., Huang, S., Ling, X. & Dresselhaus, M. S. Raman spectroscopy of transition metal dichalcogenides. *J. Phys.: Condens. Matter* **28**, 353002 (2016).
5. Full article: Polarized Raman Spectra of BaTiO<sub>3</sub>/SrTiO<sub>3</sub> Superlattices.  
<https://www.tandfonline.com/doi/full/10.1080/00150190500314833>.
6.  
  
TN199EN\_01\_A\_Polarised\_Raman\_spectroscopy\_using\_the\_inVia\_Raman\_microsc  
ope.pdf.
7. Rani, C. *et al.* Non-linear temperature dependent Raman parametric changes: An identification of Fano intervened systems. *Physics Reports* **1037**, 1–41 (2023).
8. Enhanced dielectric properties of barium strontium titanate thin films by doping modification | Journal of Materials Science: Materials in Electronics.  
<https://link.springer.com/article/10.1007/s10854-019-01670-w>.

9. Nilsen, W. G. & Skinner, J. G. Raman Spectrum of Strontium Titanate. *The Journal of Chemical Physics* **48**, 2240–2248 (1968).
10. Gray, D. J., Merz, T. A., Hikita, Y., Hwang, H. Y. & Mabuchi, H. Orientation-resolved domain mapping in tetragonal  $\text{SrTiO}_3$  using polarized Raman spectroscopy. *Phys. Rev. B* **94**, 214107 (2016).
11. Sirenko, A. A. *et al.* Observation of the First-Order Raman Scattering in  $\text{SrTiO}_3$  Thin Films. *Phys. Rev. Lett.* **82**, 4500–4503 (1999).
12. Chapman, P. W., Tufte, O. N., Zook, J. D. & Long, D. Electrical Properties of Heavily Doped Silicon. *Journal of Applied Physics* **34**, 3291–3295 (1963).
13. Balachandran, U. & Eror, N. G. Raman Spectra of Strontium Titanate. *Journal of the American Ceramic Society* **65**, c54–c56 (1982).
14. K. Saxena, S. *et al.* Amplification or cancellation of Fano resonance and quantum confinement induced asymmetries in Raman line-shapes. *Physical Chemistry Chemical Physics* **19**, 31788–31795 (2017).
15. Qualitative Evolution of Asymmetric Raman Line-Shape for NanoStructures | Silicon. <https://link.springer.com/article/10.1007/s12633-013-9176-9>.
16. Rath, D. K. *et al.* Resonant Electron–Phonon Interaction and Its Non-Fano-Type Wavelength and Power-Dependent Raman Manifestation. *J. Phys. Chem. C* **128**, 15186–15193 (2024).
17. Lineshape analysis of Raman scattering from LO and SO phonons in III-V nanowires | Journal of Applied Physics | AIP Publishing.

<https://pubs.aip.org/aip/jap/article/106/11/114317/900394/Lineshape-analysis-of-Raman-scattering-from-LO-and>.

18. M, N. K. *et al.* Size Dependent Sensitivity of Raman Line-Shape Parameters in Silicon Quantum Wire. *Advances in Materials and Processing Technologies* **6**, 669–676 (2020).
19. Kumar Rath, D. *et al.* Nonlinear Fano-Raman line-shape evolution: direct evidence of the creation and annihilation of interferons in  $V_2O_5$ . *Physical Chemistry Chemical Physics* **27**, 8674–8679 (2025).
20. Resonant Fano interaction in B1g/B3g Raman mode under off-resonant excitation in  $V_2O_5$   $\mu$ -crystals: Thermal phonon as facilitator: iScience. [https://www.cell.com/iscience/fulltext/S2589-0042\(25\)00397-9](https://www.cell.com/iscience/fulltext/S2589-0042(25)00397-9).
21. Blue- and red-shifts of  $V_2O_5$  phonons in  $NH_3$  environment by in situ Raman spectroscopy - IOPscience. <https://iopscience.iop.org/article/10.1088/1361-6463/aa98fe/meta>.

# Kuldeep Barwa\_Thesis

*by* Kuldeep Barwa

---

**Submission date:** 21-May-2025 10:41AM (UTC+0530)

**Submission ID:** 2679527985

**File name:** Master\_Thesis.pdf (1.24M)

**Word count:** 9596

**Character count:** 56600



# **Understanding Microscopic Properties of Materials Using Raman Spectroscopy**

**M.Sc. Thesis**

By  
**Kuldeep Barwa**



**Discipline of Physics**

**INDIAN INSTITUTE OF TECHNOLOGY INDORE**

**May 2025**







## INDIAN INSTITUTE OF TECHNOLOGY INDORE

### CANDIDATE'S DECLARATION

I hereby certify that the work which is being presented in the thesis entitled **Understanding Microscopic Properties of Materials Using Raman Spectroscopy** in the partial fulfillment of the requirements for the award of the degree of **MASTER OF SCIENCE** and submitted in the **DISCIPLINE OF PHYSICS, Indian Institute of Technology Indore**, is an authentic record of my own work carried out during the time period from December 2024 to May 2025 under the supervision of Professor Rajesh Kumar, Professor, Indian Institute of Technology Indore.

The matter presented in this thesis has not been submitted by me for the award of any other degree of this or any other institute.

Signature of the student with date  
(Kuldeep Barwa)

-----  
This is to certify that the above statement made by the candidate is correct to the best of my/our knowledge.

Signature of the Supervisor of M.Sc.  
thesis  
(Professor Rajesh Kumar)

-----  
Kuldeep Barwa<sup>1</sup> has successfully given his M.Sc. Oral Examination held on 14 may

Signature of Thesis Supervisor with date  
(Professor Rajesh Kumar)

*Dedicated*  
*to*  
*my Family and Teachers*

## ACKNOWLEDGEMENTS

Without the encouragement of well-wishers, a master's journey that is an emotional rollercoaster of successes is never feasible. As I write this letter to thank everyone who has been with me to support and encourage me along this journey, the two-year adventure has finally come to an end.

First and foremost, my sincerest thanks and gratitude are extended to my guide Professor Rajesh Kumar, for his guidance and motivation to complete this journey. He has been a tremendous mentor for me. His constant support, patience, valuable advice, constructive criticism, and extensive discussion helped me in accomplishing my masters. He has been inculcating inspiration, strength, knowledge, hard work, and confidence as qualities remain source of the light throughout my path of journey.

I express my sincere gratitude to Director IIT Indore, <sup>1</sup>who has been highly encouraging during the entire course of my master's <sup>2</sup>work. I would like to acknowledge all faculty members of the Physics department (IIT Indore) for their kind support and for providing me with experimental facilities. I want to thank the whole physics department which was like a family to me in these two years.

I am indebted to Deb Kumar Rath for his role as both a mentor and a friend. Her insightful advice and encouragement have been a source of motivation at every step of this endeavor.

I was lucky to spend time with my seniors Subin Kaladi Chondath, Love Bansal, Bhumika Sahu, Nikita Ahlawat, Partha S Rout, Shivam Kumar, Sharmistha Singh, Saumya Shrivastava. I would also like to thank all my batchmates and few of my good friends in IIT Indore Prashant Joshi, Arijit Paul, Harshit Dubey, Divyansh Mishra, Kartik Kohli, Faisal Ayub, Pawan Yadav, Mobashshir Mahmood for helping me and giving me joyful moments throughout this journey. I also want to thank my friends from cricket group Sonu Jaiswal, Dikku bhaiya for giving me stress-free and joyful moments. I am deeply grateful to my dear friend from beyond this campus, Jaya Sharma, for her unwavering support and kindness during my challenging times, guiding me through my journey with grace. I would also like to acknowledge Raman facilities by DST-FIST at

IIT Indore. I owe <sup>31</sup> my deepest gratitude to my parents and family for all the sacrifices they made on behalf of me and supported me in all the ups and downs of my life.



## Abstract

This thesis investigates the structural, vibrational, and electronic properties of strontium titanate, a prototypical perovskite, utilizing advanced Raman spectroscopy to elucidate its phase transitions and potential Fano effects, with significant implications for optoelectronic and energy applications. Polarized Raman spectroscopy reveals a cubic-to-tetragonal phase transition at approximately 105 K, characterized by the emergence of first-order  $B_{2g}$  modes at  $144\text{ cm}^{-1}$  and  $445\text{ cm}^{-1}$  at low temperatures (93 K and 88 K), with polarization-dependent intensity variations confirming tetragonal domain alignment and anisotropic vibrational properties, underscoring  $\text{SrTiO}_3$ 's quantum paraelectric behaviour, though local strains indicate areas for further exploration. Additionally, the study explores potential Fano resonance in STO's low-frequency  $\text{TO}_2$ -TA mode, which exhibits asymmetric line shapes suggestive of quantum interference, drawing comparisons with established Fano effects in heavily doped silicon ( $520\text{ cm}^{-1}$  peak) and vanadium pentoxide ( $995\text{ cm}^{-1}$  Ag mode), where temperature-dependent asymmetries and photoexcitation amplify nonlinear behaviours. While anharmonic phonon interactions in  $\text{SrTiO}_3$  hinder definitive Fano confirmation, a framework leveraging silicon and vanadium pentoxide's nonlinear properties is proposed to investigate Fano effects in complex oxides, enhancing understanding of sample's low-temperature dynamics and its potential in oxide electronics. The developed temperature-dependent and polarized Raman methodologies provide a robust approach for studying perovskites, offering valuable insights for optimizing materials in solar cells, microelectronics, and catalysis.

## List of Publications



## List of Figures

<b>Figure 1.1:</b> General structure of perovskites.	19
<b>Figure 1.2:</b> Sir C.V. Raman with the very first setup of the Raman spectrometer (image courtesy, IISc Bangalore).	21
<b>Figure 1.3:</b> Schematic shows the function of the Fano resonance.	23
<b>Figure 1.4:</b> Schematic represents the effect of different perturbations on the Raman spectra.	23
<b>Figure 2.1:</b> General structure of Strontium Titanate.	26
<b>Figure 2.2:</b> Raman spectrum of STO for (a) room temperature and (b) at 93 K.	28
<b>Figure 2.3:</b> (a) Polarization dependent Raman spectra of SrTiO <sub>3</sub> at 93 K from 0 degree to 360 degree showing the first order Raman modes about 144 cm <sup>-1</sup> and 445 cm <sup>-1</sup> and (b) Zoomed version of figure a showing the variation of intensity of B <sub>2g</sub> mode at 144 cm <sup>-1</sup> from 0 degree to 360 degree.	29
<b>Figure 2.4:</b> Polar plot of intensity variation of B <sub>2g</sub> Raman mode (144 cm <sup>-1</sup> ) as function of polarization angle $\theta$ at 93 K with 633 nm laser.	31
<b>Figure 2.5:</b> Polar plot of intensity variation of B <sub>2g</sub> Raman mode (144 cm <sup>-1</sup> ) as function of polarization angle $\theta$ at 88 K with 532 nm laser.	32
<b>Figure 3.1:</b> (a) The temperature dependent Raman spectrum of Strontium Titanate showing the low frequency mode (TO <sub>2</sub> -TA) about 80cm <sup>-1</sup> and the zoomed version of this mode is plotted (fig b) using 532 nm laser.	38
<b>Figure 3.2:</b> Variation in Raman peak-position with temperature for STO sample and Variation in Linewidth with temperature is plotted.	39

**Figure 3.3** <sup>4</sup> Temperature dependent Raman spectra from heavily doped p type Si using 532 nm laser for <sup>60</sup> the peak at 520  $\text{cm}^{-1}$ . 41

**Figure 3.4:** Variation in the Fano parameter, peak position and line width is plotted respectively as the temperature changes for the peak 520  $\text{cm}^{-1}$ . 42

**Figure 3.5:** Temperature dependent Raman spectrum of  $\text{V}_2\text{O}_5$  material for the peak 995 <sup>9</sup>  $\text{cm}^{-1}$  and the zooming version of 995  $\text{cm}^{-1}$  (in the inset). 44

**Figure 3.6:** Variation in the Fano parameter, peak position and line width is plotted respectively as the temperature changes for the peak 995  $\text{cm}^{-1}$ . 45



# Contents

Acknowledgement	6
Abstract	8
<sup>33</sup> List of Publications	9
List of Figures	10
Chapter 1: Introduction	18
Chapter 2: Phase Transition in Strontium Titanate	25
2.1 Why Strontium Titanate:	
2.3 Literature study:	
2.3 Experimental Details:	
2.4 Results and Discussions:	
2.5 Summary:	
Chapter 3: Fano Effect Explored in Different Materials	35
3.1 Nonlinear Phonon behaviour in Heavily Doped Semiconductor Si and V <sub>2</sub> O <sub>5</sub>	
<sup>32</sup> 3.2 Temperature-Dependent Raman Spectra of Strontium Titanate:	

3.3 Temperature dependent Raman Spectra of heavily doped Silicon (Si) material:

3.4 Temperature dependent Raman spectrum of  $V_2O_5$  material:

3.5 Summary:

**Chapter 4: Conclusion** 49

**References** 51





# Chapter 1

## Introduction

Perovskites<sup>20</sup> have emerged as a fascinating class of materials in materials science and condensed matter physics, capturing significant attention due to their versatile properties and potential applications in optoelectronic devices.<sup>52</sup> Named after the mineral perovskite ( $\text{CaTiO}_3$ ), these materials share a characteristic crystal structure defined by the general formula  $\text{ABX}_3$ .<sup>15</sup> In this structure, A and B are cations of different sizes, and X is an anion, typically oxygen or a halide.<sup>12</sup> The A cation is usually a larger organic or inorganic ion (e.g., methylammonium, cesium), B is a smaller metal cation (e.g., lead, tin), and X is often a halide (e.g., iodide, bromide) or oxide. This structural flexibility allows perovskites to exhibit a wide range of physical and chemical properties, making them highly tunable for applications such as solar cells, light-emitting diodes (LEDs), photodetectors, and lasers.<sup>37</sup>

Perovskites are particularly notable for their semiconductor properties<sup>1</sup>, which make them promising candidates for next-generation electronic and optoelectronic technologies.<sup>43</sup> A semiconductor is a material with electrical conductivity between that of insulators and conductors, governed by its band gap—the energy difference between the valence and conduction bands.<sup>36</sup> Semiconductors can be intrinsic, where conductivity arises from the material's inherent properties, or extrinsic, where conductivity is enhanced by doping with impurities. The ability to control charge carrier behaviour in semiconductors underpins modern electronics, including transistors, diodes, and photovoltaic devices.<sup>35</sup> Perovskites, as semiconductors, stand out due to their high charge carrier mobility, long carrier diffusion lengths, and tunable band gaps,<sup>29</sup> which can be adjusted by varying the composition of A, B, or X ions.



The optical and electronic properties<sup>2</sup> of perovskites are central to their technological relevance. Optically, perovskites exhibit strong light absorption across a broad spectral range, high photoluminescence quantum yields, and efficient emission, making them ideal for photovoltaic and light-emitting applications. Their band gap can be tailored by substituting halides (e.g., mixing iodide and bromide) or cations, enabling precise control over the wavelengths of light they absorb or emit. Electronically, perovskites possess excellent charge transport properties<sup>38</sup>, with low defect densities and high carrier lifetimes, which enhance the efficiency of devices like solar cells. For instance, lead-halide perovskites have achieved power conversion efficiencies exceeding 25% in solar cells, rivalling traditional silicon-based technologies. Additionally, their ambipolar charge transport—allowing efficient movement of both electrons and holes—further enhances their versatility.

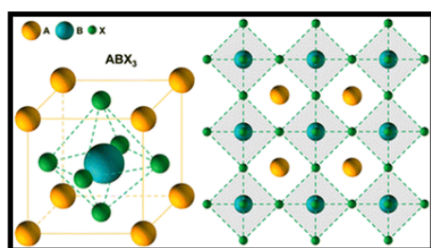


Figure 1.1: General structure of perovskites<sup>3</sup>

Raman spectroscopy serves as a powerful, non-destructive technique for probing the microscopic properties of perovskites, offering detailed insights into their structural and vibrational characteristics. Discovered in 1928 by Sir C.V. Raman and K.S. Krishnan, the Raman effect describes the inelastic scattering of light by matter, where incident photons interact with molecular vibrations or lattice phonons, resulting in a shift in the scattered light's energy. This energy shift, known as the Raman shift, provides a unique fingerprint of the material's vibrational modes, revealing information about its chemical composition, crystal structure, and lattice dynamics. Raman spectroscopy's discovery<sup>28</sup> earned Sir C.V. Raman the Nobel Prize in Physics in 1930, marking a significant milestone in

materials characterization. Unlike other <sup>42</sup> techniques, such as X-ray diffraction (XRD) or infrared (IR) spectroscopy, Raman spectroscopy offers several distinct advantages. It requires minimal sample preparation, is highly sensitive to subtle changes in molecular and lattice structures, and can be performed under ambient conditions without damaging the sample. Compared to IR spectroscopy, which probes dipole moment changes, Raman spectroscopy detects changes in polarizability, providing complementary information about vibrational modes, particularly for symmetric bonds. Raman spectroscopy excels in studying low-frequency lattice vibrations, critical for understanding phase transitions and structural stability in perovskites. Its ability to spatially resolve features at the micrometre scale, especially in confocal Raman setups, further

distinguishes it from techniques like photoluminescence spectroscopy, which primarily focus on electronic transitions. By leveraging Raman spectroscopy, this thesis investigates the microscopic properties of perovskites, including their lattice dynamics, phase behaviour, and molecular interactions, to elucidate the fundamental mechanisms governing their optoelectronic performance. This work aims to advance the understanding of perovskite-based materials for sustainable energy and advanced electronic applications.

Temperature-dependent Raman spectroscopy and polarized<sup>4</sup> Raman spectroscopy further enhance the capability of Raman techniques in studying perovskites. Temperature-dependent Raman spectroscopy involves measuring Raman spectra at varying temperatures to probe the material's response to thermal changes, offering insights into phase transitions, lattice dynamics, and anharmonic interactions. In perovskites, temperature variations can induce structural phase transitions (e.g., from cubic to tetragonal or orthorhombic phases), which alter vibrational modes and are reflected in shifts or broadening of Raman peaks. This technique is particularly valuable for understanding thermal stability and lattice anharmonicity, which influence the optoelectronic performance of perovskites in real-world applications.

Polarized Raman spectroscopy<sup>5</sup> is a specialized technique that enhances the study of vibrational properties in crystalline materials like perovskites by exploiting the polarization of light to probe the symmetry and orientation of vibrational modes. Unlike conventional Raman spectroscopy, which measures the inelastic scattering of light to reveal a material's vibrational fingerprint, polarized Raman spectroscopy controls the polarization of both the incident and scattered light to extract detailed information about the crystal's anisotropic properties. In this method, two primary configurations are used: parallel polarization, where the incident and scattered light polarizations<sup>6</sup> are aligned (e.g., both along the same crystal axis), and cross-polarization, where they are perpendicular (e.g., incident light polarized along one axis and scattered light along an orthogonal axis). The intensity of Raman peaks in these configurations is governed by the Raman tensor, a mathematical representation of how a vibrational mode interacts with polarized light. The Raman tensor, specific to each vibrational mode, depends on the crystal's symmetry and determines which modes are active or suppressed under different polarization conditions. For instance, in a perovskite like SrTiO<sub>3</sub>, the tensor's components reflect the cubic or tetragonal symmetry, influencing the observed Raman intensities. By

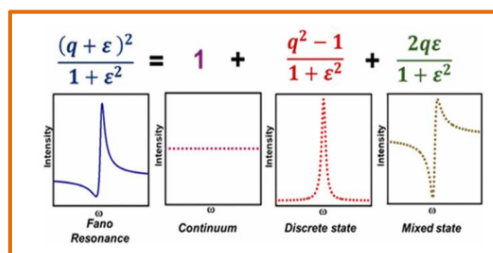


Figure 1.2: Sir C.V. Raman with the very first setup of the Raman spectrometer (image courtesy, IISc Bangalore)

<sup>22</sup> rotating the polarization angle of the incident or scattered light relative to the crystal axes, the intensity of Raman peaks varies, often following a sinusoidal pattern that reveals the mode's symmetry and the crystal's structural orientation.

This intensity variation can be visualized in polar plots, which map the Raman signal as a function of polarization angle, providing a direct way to characterize anisotropic vibrational behaviour.<sup>2</sup> Polarized Raman spectroscopy<sup>7</sup> is particularly powerful for studying phase transitions in perovskites, as changes in crystal symmetry (e.g., from cubic to tetragonal) alter the Raman tensor, leading to distinct intensity patterns in parallel and cross-polarized spectra. This technique thus offers a window into the microscopic lattice dynamics and structural properties critical for understanding the optoelectronic performance of perovskite materials.

In materials like perovskites, which undergo phase transitions with temperature or exhibit strong electron-phonon interactions, these deviations arise because thermal perturbations and phase changes introduce asymmetries in Raman peak shapes. Beyond thermal and confinement effects, phenomena such as doping or electron-phonon coupling, notably the Fano effect, significantly influence Raman spectra. The Fano effect, first described by Ugo Fano in 1961, occurs when a discrete vibrational mode (e.g., a phonon in Raman spectroscopy) interferes with a continuum of electronic states, resulting in asymmetric peak shapes and, in some cases, antiresonance features in the spectra. In perovskites, this electron-phonon interaction is pronounced due to their semiconductor nature, where free carriers interact strongly with lattice vibrations. Unlike thermal effects, which broaden peaks uniformly with rising temperature, doping introduces distinct perturbations by altering carrier concentrations, leading to unique changes in Raman line shapes. Temperature-dependent Raman spectroscopy is crucial for tracking these Fano-induced asymmetries as thermal energy modifies electron-phonon coupling, while polarized Raman spectroscopy, as employed in this study, reveals how these asymmetries depend on crystal orientation and vibrational symmetry. Schematic figures<sup>7</sup> are given below for Fano effect.



41  
Figure 1.3: Schematic shows the function of the Fano resonance.

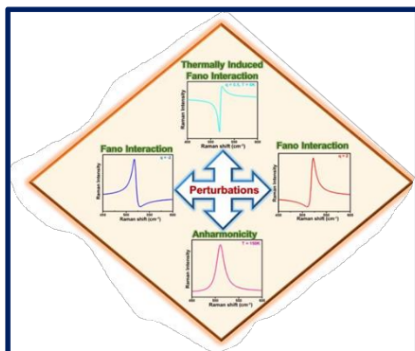


Figure 1.4: Schematic represents<sup>7</sup> the effect of different perturbations on the Raman spectra.



## Chapter 2

62

### Phase Transition in Strontium Titanate

This chapter investigates the phase transition of single-crystal strontium titanate (STO) using Polarized Raman Spectroscopy. As the material undergoes a phase transition, Raman spectra were collected at room temperature and below 105 K. The sharp peak in the spectra indicates a phase change, and this study explores how the intensity of this peak varies with temperature and angle. Using group theory, the Raman tensor for  $B_{2g}$  mode observed in the Raman spectrum is analysed. The  $B_{2g}$  mode at  $144\text{ cm}^{-1}$  is examined by calculating its intensity at temperatures of 93 K and 88 K, and a polar plot of intensity versus angle was calculated to further characterize the phase transition behaviour.

#### 2.1 Why Strontium Titanate:

Single-crystal strontium titanate ( $\text{SrTiO}_3$ ) is a perovskite material known for its highly ordered crystal structure and unique phase transition properties, making it a cornerstone for studying lattice dynamics. STO exhibits quantum paraelectric behaviour, undergoing a structural phase transition at low temperatures (around 105 K) driven by soft phonon modes, without developing full ferroelectric polarization. This transition, sensitive to temperature and strain, highlights its dynamic perovskite characteristics. Decades of research, from foundational studies in the 1960s to recent explorations of its interfaces, have revealed STO's exceptional dielectric properties, superconductivity, and ability to host two-dimensional electron gases. These attributes make STO invaluable for applications such as tunable capacitors, ferroelectric technologies, and oxide electronics. The single-crystal form ensures minimal defects and uniform properties, providing a reliable platform for investigating the fundamental physics and technological potential of perovskites. Raman spectroscopy is an effective method for identifying transitions in these materials. However, in  $\text{SrTiO}_3$ , the emergence of second-order multi-phonon Raman signals complicates the

understanding of the mechanism. Scientists have employed many methodologies and methods to address the confusion linked to Raman effects. It is intriguing to comprehend the process of structural phase transition from cubic to tetragonal through the analysis of Raman spectra.

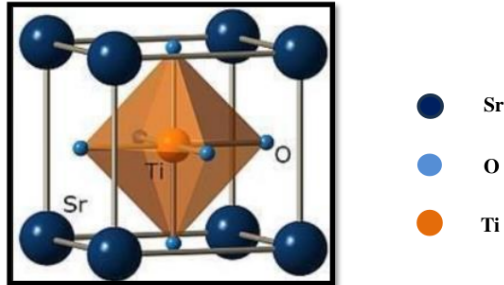


Figure 2.1: General structure of Strontium Titanate<sup>8</sup>

## 2.2 Literature study:

(i) The Raman spectrum of single-crystal  $\text{SrTiO}_3$ , as studied by W. G. Nilson<sup>9</sup> et al., reveals key insights into its phase transitions with temperature, down to 25 K. At room temperature, the spectrum is entirely second-order, consistent with the cubic perovskite structure, with phonons near the Brillouin zone boundary, mostly transversely polarized. Upon cooling below the 110 K phase transition, STO exhibits three sharp lines from local modes, not polar transverse-optic (TO) modes, indicating a structural change. This highlights Raman scattering's sensitivity to crystal structure, showing distinct phase transitions in STO. The tetragonal phase of  $\text{SrTiO}_3$  likely has a  $C_{4h}$  point group, as no ferroelectricity or first-order Raman scattering is observed.

(ii) Dodd J. Gray et al.<sup>10</sup>, conducted microscopically resolved polarized Raman spectroscopy on tetragonal  $\text{SrTiO}_3$ , focusing on the anisotropic response of first-order Raman peaks within a single tetragonal domain. Their work enabled symmetry assignments to phonons in the first-order Raman spectrum, which is typically obscured by complex, uncontrolled domain structures. By using a translation stage, they mapped



the local domain orientation in a  $3\text{-}\mu\text{m}^3$  crystal volume near the laser focus, comparing these results to wide-field polarized images. This method, leveraging standard instruments, is versatile and applicable to studying related materials, interfaces, and devices.

(iii) A.A. Sirenko et al<sup>11</sup>, conducted the Raman spectrum of  $\text{SrTiO}_3$ , measured at room temperature, reveals patterns linked to second-order scattering, mainly at the Brillouin zone boundary. By examining the energy shifts, researchers determined the single-phonon energies for ten distinct phonon branches used to identify spectral peaks. A new finding is an impurity-related band at  $793\text{ cm}^{-1}$ , observed at 120 K in the tetragonal phase. Impurities in the  $\text{SrTiO}_3$  sample also raised the temperature of the cubic-to-tetragonal phase transition to around 120 K. These energy shifts match well with prior single-crystal studies, confirming the reliability of the results. This echoes Burns and Scott's work on  $\text{PbZr}_x\text{Ti}_{1-x}\text{O}_3$ , which noted that while single crystals offer detailed insights, powder samples can provide much of the same information in some cases.

By taking the references of these literatures and more, the experiment is done on the STO to analyze the intensity variation and confirm the phase change below room temperature from cubic to tetragonal structure.

### 2.3 Experimental Details:

The commercially procured Strontium titanate ( $\text{SrTiO}_3$ ) single crystal (001) has been used for Raman measurement. The Horiba-Jobin Yvon LABRAM-HR spectrometer was used to perform the Raman spectroscopy measurement using excitation wavelengths of 633 nm and 532 nm. Using a 50X long working distance objective and a Linkam stage, the TD Raman measurements were performed at the temperature of 93 K and 88 K. The temperature was held and the sample was manually focused. The spectrometer's integrated software was utilized to adjust the temperature, along with a temperature controller. The polarization dependent measurement has been done by introducing the polarizer in the direction of incident light and an analyzer in the direction of scattered light. The axis of polarization can be rotated by angle 0 to 360

degree by a half wave plate ( $\lambda/2$ ), while the position of the axis of analyzer is fixed. The angle variation is taken the difference of 10 degree. we locally probed the symmetry of one Raman-active ( $B_{2g}$ ) phonon mode. Micro-Raman experiments on  $\text{SrTiO}_3$  require higher excitation powers and longer exposure times compared to materials like graphene due to its 3.2-eV band-gap energy, which is significantly above the 2.33-eV excitation photon energy. That's why the low frequency mode will disappear in 633 nm laser light.

## 2.4 Results and Discussions:

The Raman spectra has been recorded at room temperature and at 93 K at parallel polarization configuration. The Spectrum of  $\text{SrTiO}_3$  at 93 K shows two sharp peaks at about  $144 \text{ cm}^{-1}$  and  $445 \text{ cm}^{-1}$ .

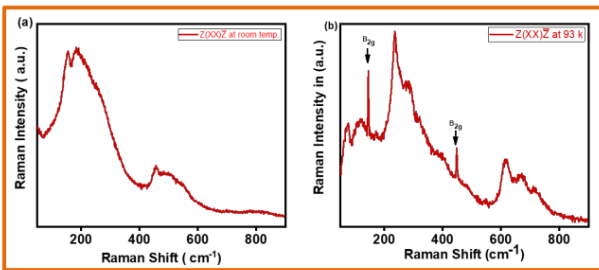


Figure 2.2: Raman spectrum of STO for (a) room temperature and (b) at 93 K

These are the first order Raman modes having symmetry  $B_{2g}$ . These Raman modes can be seen only because of tetragonal phase transition of  $\text{SrTiO}_3$  from cubic phase at low temperature. These Raman modes can be seen only because of tetragonal phase transition of  $\text{SrTiO}_3$  from cubic phase at low temperature. These modes emerge due to the tetragonal phase, which breaks the cubic symmetry and allows first-order scattering. The phase transition is driven by soft phonon modes, particularly the polar transverse-optic modes, which soften (decrease in frequency) as temperature drops,

destabilizing the cubic phase and facilitating the transition to the tetragonal phase. These soft modes play a critical role in the structural rearrangement, enabling the observation of  $B_{2g}$  modes at 93 K, while the <sup>18</sup>second-order scattering at room temperature reflects the harmonic combinations of phonons in the cubic phase.

The Raman mode obeying  $B_{2g}$  symmetry of tetragonal phase are <sup>44</sup>strongly dependent on the polarization of the electric field incident and provides a lot of information about the tetragonality of the crystal structure. So, a polarization dependent Raman measurement has been done at 93 K by rotating the linearly polarized incident light from 0 degree to 360 degree (Figure a and b).

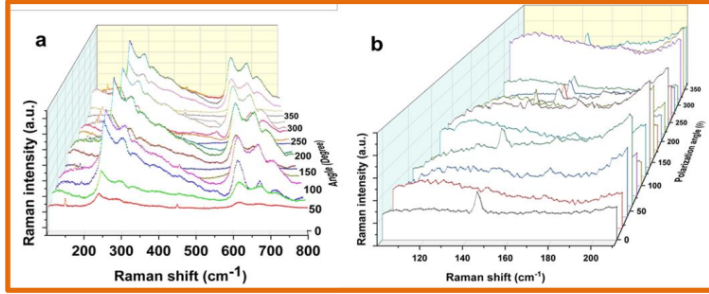





Figure 2.3: (a) Polarization dependent Raman spectra of  $\text{SrTiO}_3$  at 93 K from 0 degree to 360 degree showing the first order Raman modes about  $144 \text{ cm}^{-1}$  and  $445 \text{ cm}^{-1}$  and (b) Zoomed version of figure a showing the variation of intensity of  $B_{2g}$  mode at  $144 \text{ cm}^{-1}$  from 0 degree to 360 degree.

To understand <sup>2</sup>the tetragonal phase orientation of  $\text{SrTiO}_3$ , the polarization dependent of  $B_{2g}$  Raman mode at  $144 \text{ cm}^{-1}$  has been analyzed as per the mathematical Raman tensor analysis as following way. Since the in transition, the tetragonal axis (c-axis) transition can be happened along any arbitrary direction as the temperature is lowered, it is interesting to investigate the tetragonal domain orientation at a particular temperature and how it changes as the temperature varies.

The phase transition in SrTiO<sub>3</sub> from a cubic to a tetragonal structure, occurring around 110 K, is driven by the softening of an R-point optical phonon, which reduces to zero frequency, lowering the crystal symmetry from the O<sub>h</sub> to the D<sub>4h</sub> point group. This structural change involves elongation of the unit cell along the tetragonal axis, a 45° rotation, and an expansion by a factor of  $\sqrt{2}$  in the basal plane dimensions. At room temperature, the cubic phase restricts Raman scattering to second-order processes due to symmetry selection rules, producing broad spectra from phonon combinations. Upon cooling to 93 K, below the phase transition, the tetragonal phase enables first-order Raman scattering, with distinct B<sub>2g</sub> symmetry modes observed at approximately 144 cm<sup>-1</sup> and 445 cm<sup>-1</sup> in parallel polarization configuration. Additional phonon modes with A<sub>1g</sub>, B<sub>1g</sub>, and E<sub>g</sub> symmetries also become Raman-active in this phase. The intensity of the B<sub>2g</sub> modes varies with the polarization angle  $\theta$  and the orientation of the tetragonal axis (along X, Y, or Z), reflecting the domain structure. The softening of the R-point phonon is critical, as it destabilizes the cubic lattice, facilitating the transition and enabling the emergence of first-order Raman signals characteristic of the tetragonal phase. The relative strength of the Raman response as a function of polarization angle  $\theta$ ,  $I_{ij}(\theta)$ , for B<sub>2g</sub> symmetry and Tetragonal axis domain orientation  $j \in \{X, Y, Z\}$  has been mentioned.

**Table 1: The two-dimensional quasi cubic Raman tensor of B<sub>2g</sub> symmetry in all possible direction of x y and z.<sup>10</sup>**

Raman tensor	$I_x, c  x$	$I_y, c  y$	$I_z, c  z$				
$B_{2g}$ (145 cm <sup>-1</sup> , 448 cm <sup>-1</sup> )	$\begin{bmatrix} 0 & d & 0 \\ d & 0 & 0 \\ 0 & 0 & 0 \end{bmatrix}$	$\begin{bmatrix} 0 & 0 \\ 0 & d \end{bmatrix}$	$d^2 \sin^4(\theta)$ 	$\begin{bmatrix} d & 0 \\ 0 & 0 \end{bmatrix}$	$d^2 \cos^4(\theta)$ 	$\begin{bmatrix} -d & 0 \\ 0 & d \end{bmatrix}$	$d^2 \cos^2(2\theta)$ 

In a cubic structure, the unit cell parameters are equal, (a = b = c) but a change of lattice parameter to (a = b  $\neq$  c) after a phase transition to a tetragonal structure happened as mentioned earlier. Since the tetragonal axis (c) can be elongated in any

arbitrary axis of x, y, or z (if assumed to be aligned in a, b and c axis of unit cell), this can be resolved from the above intensity calculation of polarization tensor (Table 1).

From figure 2.3b the integrated intensity of  $B_{2g}$  Raman mode at  $144 \text{ cm}^{-1}$  has been plotted as a function of polarization angle  $\theta$  in polar plot as shown in figure 2.4. It is clear from the plot that it follows the intensity variation  $I_z(\theta)$  as  $d^2 \cos^2(2\theta)$ , where d is the Raman tensor element of  $B_{2g}$  symmetry. Since the maximum intensity of the polar plot (figure 2.4) is not exactly at 90, 180 and 270 degrees so the tetragonality changes initiated along the z axis in the domain where laser is focused in the single crystal.

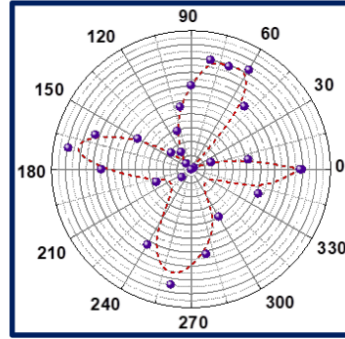


Figure 2.4: Polar plot of intensity variation of  $B_{2g}$  Raman mode ( $144 \text{ cm}^{-1}$ ) as function of polarization angle  $\theta$  at 93 K with 633 nm laser.

It will be interesting to investigate the detail transition of tetragonality as the temperature is lowered. STO is a well-known perovskite with a large band gap ( $\sim 3.2 \text{ eV}$ ), requiring high-energy excitation like a 532 nm laser ( $\sim 2.33 \text{ eV}$ ) to probe its vibrational modes effectively. So, the same experiment is done by cooling the sample by 88 K from a reference temperature for  $B_{2g}$  mode. It can reveal how the tetragonal structure evolves and whether the c-axis undergoes changes in alignment or tetragonality (fig 2.5).

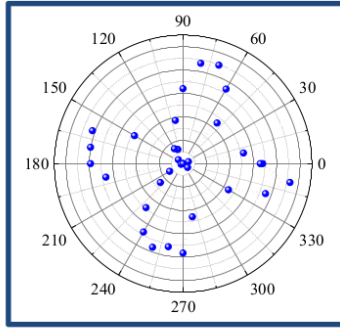


Fig 2.5: Polar plot of intensity versus polarization angle  $\theta$  of  $B_{2g}$  Raman mode ( $144 \text{ cm}^{-1}$ ) as function of polarization angle  $\theta$  at 88 K with 532 nm laser.

polar plots for the  $B_{2g}$  Raman mode at  $144 \text{ cm}^{-1}$  at 93 K (633 nm laser) and 88 K (532 nm laser), suggesting that tetragonality is independent of laser wavelength in this temperature range, though intensity may vary with frequency. STO undergoes a cubic-to-tetragonal phase transition at  $\sim 105 \text{ K}$ , and at 93 K and 88 K, it is already in the tetragonal phase, characterized by oxygen octahedra rotations. Lowering the temperature further may enhance the tetragonal distortion and stabilize the low-temperature phase.

The angular pattern of the  $B_{2g}$  Raman mode should stay the same unless a higher-energy laser triggers changes in the crystal's electronic or structural properties. The polar plot's shape depends on the Raman tensor, which reflects the tetragonal symmetry and isn't affected by the laser's frequency. The tetragonal structure and  $c/a$  ratio are determined by the crystal's lattice and temperature, not the laser's wavelength. Therefore, using a higher-frequency laser shouldn't directly change the tetragonality. However, lasers with wavelengths close to the band gap, like 405 nm, might cause minor photoinduced effects that subtly influence the crystal's behaviour.

## 2.5 Summary:

Raman spectroscopy on a  $\text{SrTiO}_3$  (001) single crystal revealed first-order  $B_{2g}$  modes at  $144\text{ cm}^{-1}$  and  $445\text{ cm}^{-1}$  at 93 K, confirming a cubic-to-tetragonal transition ( $\sim 105\text{ K}$ ) driven by soft R-point phonons, enabling first-order scattering in the  $D_{4h}$  symmetry phase. The  $144\text{ cm}^{-1}$  mode's intensity, varying as  $d^2\cos^2(2\theta)$  with polarization angle, indicated z-axis-aligned tetragonal domains. Polar plots at 93 K (633 nm) and 88 K (532 nm) showed consistent tetragonality and increased c/a ratio, but maxima shift from  $90^\circ$ ,  $180^\circ$ , and  $270^\circ$  suggested strain or domain misalignment. At lower temperatures, the  $B_{2g}$  mode in  $\text{SrTiO}_3$  shows a stronger intensity, and the polar plot displays sharper peaks, indicating a more pronounced angular dependence. Using a higher-frequency laser boosts the overall intensity further, making these angular patterns even clearer. The tetragonal symmetry of the material remains stable, with the c/a ratio (the ratio of the lattice parameters along the c and a axes) increasing as temperature drops, reflecting a stronger tetragonal distortion. Importantly, the shape of the polar plot stays consistent across different laser frequencies, confirming that the material's tetragonality is not influenced by the laser frequency. This aligns with observations at 93 K and 88 K, where the tetragonal phase was robust.

However, the intensity maxima in the polar plot are not aligned at the expected angles of  $90^\circ$ ,  $180^\circ$ , and  $270^\circ$ . This misalignment suggests the presence of local strain, defects, or misaligned domains in the sample, which persist regardless of temperature or laser frequency. Lowering the temperature might reduce these angular shifts if they are caused by thermal vibrations or dynamic disorder, as thermal effects diminish at colder conditions. However, if the shifts persist, it points to structural defects or static strain, possibly tied to the sample's powder nature, as discussed in the prior summary where powder samples yielded results comparable to single crystals. To summarize, the increased  $B_{2g}$  mode intensity and sharper polar plot maxima at lower temperatures, amplified by higher-frequency lasers, highlight the robust tetragonal symmetry and increased c/a ratio in  $\text{SrTiO}_3$ . The consistent polar plot shape across laser frequencies supports the independence of tetragonality from laser effects, while the misaligned

intensity maxima suggest ongoing local strain or defects, potentially linked to impurities or domain issues, which may or may not lessen with further cooling.



## Chapter 3

### Fano Effect Explored in Different Materials

<sup>22</sup> Raman spectroscopy has long been a powerful tool for studying the vibrational properties of materials, but some of its most interesting features appear when we look beyond simple symmetric peaks. The Fano effect, studied in the chapter 1, that distinctive asymmetric line shape that appears in spectra tells that when phonons are interacting with electronic excitations in the material. While this phenomenon has been thoroughly documented in materials like silicon and vanadium pentoxide, its presence in strontium titanate ( $\text{SrTiO}_3$ ) remains less clear, despite the material's interesting properties and technological importance.

What makes this material particularly fascinating is how its properties change with temperature. As the material is cooled, it doesn't undergo a typical ferroelectric transition, but instead enters what we call a quantum paraelectric state. This strange behaviour shows up in its phonon modes too, especially in the famous "soft mode" that becomes unstable at low temperatures. The work focuses on whether these unusual phonons might be interacting with electrons to produce Fano resonances, and how these interactions evolve across different temperature regimes.

In this chapter, the detailed temperature-dependent Raman studies of  $\text{SrTiO}_3$ , tracking how the line shapes change as we vary the temperature from room temperature down to cryogenic ranges. The measurements are designed to catch any signs of Fano interference, particularly in the spectral regions where we expect strong electron-phonon coupling. To help interpret these results, the data will be compared with measurements from silicon and vanadium pentoxide, two materials where Fano effects are well established. The Fano effect manifests distinctly in different material systems. In silicon, the Fano resonance arises from the interaction between optical phonons and free carriers in doped samples, producing characteristic asymmetric line shapes in the first-order Raman spectrum near  $520\text{ cm}^{-1}$ . This phenomenon has been extensively studied since the 1970s, with the Fano parameter  $q$  quantitatively describing the

<sup>5</sup> coupling strength between discrete phonon modes and the electronic continuum.

Vanadium pentoxide presents a more complex case, where Fano asymmetries emerge from interactions between lattice vibrations and continuum states associated which is due to photoexcitation which is called resonant Raman scattering and particularly studied in this chapter for the  $995\text{ cm}^{-1}$  region.  $\text{V}_2\text{O}_5$ 's Raman spectra reveal pronounced Fano line shapes that vary with temperature and stoichiometry, reflecting the strong electron-phonon coupling inherent to this transition metal oxide. The motivation behind this work goes beyond just cataloguing another material that shows Fano resonance. Understanding these effects in  $\text{SrTiO}_3$  could give new insights into its peculiar low-temperature behaviour and help explain some of its unusual properties. From a practical perspective, since  $\text{SrTiO}_3$  serves as the foundation for many oxide heterostructures and interfaces, knowing how its phonons interact with electrons could be important for future device applications. This study aims to provide clear evidence for or against Fano resonance in STO, while developing methods that could be applied to other complex oxides.

### 3.1 Nonlinear Phonon behaviour in Heavily Doped Semiconductor Si and $\text{V}_2\text{O}_5$ :

In heavily doped semiconductor  $\text{Si}^{12}$ , an elevated concentration of charge carriers—electrons or holes—triggers significant interactions with the crystal lattice, leading to a proliferation of lattice vibrations, known as phonons, particularly at the boundaries of the material's vibrational zones. These phonons accumulate because their generation outpaces their natural, anharmonic decay, and as temperature increases, this decay becomes nonlinear, intensifying the dynamics. Some phonons form bound states with charge carriers, potentially giving rise to quasiparticles or interference effects, possibly what was referred to as “interferons” in this context. This environment creates fertile ground for the Fano effect, a quantum phenomenon where <sup>61</sup> a discrete energy state interferes with a continuum of states, provided their energies align, producing distinctive asymmetric spectral features detectable through spectroscopic methods. This interference arises from <sup>4</sup> two competing pathways: one linking the ground state to

a specific excited nonlinear form, the Fano effect becomes more complex, driven by strong perturbations, as observed in hybrid systems like metal nanoparticles combined with semiconductor quantum dots. Importantly, no thermodynamic constraints prevent this nonlinear Fano effect from occurring in semiconductors, provided the energy conditions are met and appropriate external stimuli are applied. Given the critical role of semiconductors in technologies such as microelectronics and photovoltaics, investigating this phenomenon is highly compelling. To induce the nonlinear Fano effect, one could apply intense laser pulses to generate excitons or plasmons that couple with phonons, or employ ultrafast laser techniques to capture transient interference states. Strong electric or magnetic fields could modulate the material's energy structure, while elevated temperatures or tailored modifications, such as mechanical strain or precise doping, could align the discrete and continuum energy levels. By leveraging advanced spectroscopy to detect characteristic asymmetric spectral signatures or monitoring time-resolved signals following laser excitation, researchers could probe the presence of the nonlinear Fano effect, potentially unlocking new insights into the behavior of these essential materials.

Transition metal oxides, particularly vanadium pentoxide ( $V_2O_5$ ), are widely studied for their unique electronic, structural, and chemical properties, driven by d-electrons and their versatility in catalytic and electrochemical applications.  $V_2O_5$ , stable in its  $V^{+5}$  oxidation state, is theoretically an insulator but exhibits weak vanadyl oxygen bonding, enabling applications in solar cells, antireflection coatings, and electrochromic devices. Its electronic and vibrational properties are well-documented, yet microscopic phenomena like electron-phonon interactions in bulk  $V_2O_5$  remain underexplored. The Ag Raman mode of  $V_2O_5$  powder displays asymmetry and an antiresonance dip, indicative of electron-phonon interactions, supported by a noticeable electronic Raman background. This mode aligns with the Fano-Raman equation, but laser power and wavelength variations reveal a resonant Fano interaction, weakening at higher laser power, unlike typical Fano systems such as heavily doped silicon. Wavelength-dependent Raman scattering further confirms the resonant nature, highlighting photoexcitation's role when laser energy exceeds the band gap, offering insights into  $V_2O_5$ 's vibrational dynamics.

### 3.2 Temperature-Dependent Raman Spectra of Strontium Titanate:

The temperature-dependent Raman spectrum of single-crystal  $\text{SrTiO}_3$  (STO) was obtained using a 532 nm laser. While low-frequency modes were absent in spectra collected with a low frequency laser, these modes, particularly the  $\text{TO}_2\text{-TA}$  mode<sup>13</sup>, were observed with the 532 nm laser. This low-frequency mode exhibits an asymmetric line shape that varies with temperature, suggesting a may be possible Fano effect. The presence of an electronic background and an antiresonance dip further supports this hypothesis. The  $\text{TO}_2\text{-TA}$  mode typically appears in the low-frequency region of STO's Raman spectrum, often below  $\sim 100 \text{ cm}^{-1}$ , depending on experimental conditions. In STO, a perovskite known for its incipient ferroelectricity and quantum paraelectric behaviour, low-frequency modes like  $\text{TO}_2\text{-TA}$  are associated with soft phonons that drive structural phase transitions, such as the cubic-to-tetragonal transition at  $\sim 105 \text{ K}$ .

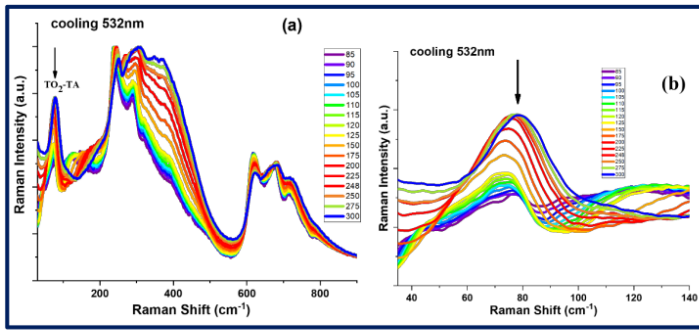


Figure 3.1 (a) The temperature dependent Raman spectrum of Strontium Titanate showing the low frequency mode ( $\text{TO}_2\text{-TA}$ ) about  $80 \text{ cm}^{-1}$  and the zoomed version of this mode is plotted (fig b) using 532 nm laser.

45 The observed asymmetry in the Raman line shape of the TO<sub>2</sub>-TA mode in single-crystal SrTiO<sub>3</sub>, measured using a 532 nm laser, cannot be immediately attributed to the Fano effect without thorough investigation, as multiple phenomena could contribute to such spectral features. To accurately 5 determine whether the asymmetry arises from a Fano interaction—characterized by interference between a discrete phonon mode and a continuum of electronic states—or from other mechanisms, a detailed analysis of the Raman spectra is essential. Potential alternative phenomena include anharmonic phonon-phonon interactions, disorder-induced broadening, or contributions from overlapping modes, each of which could mimic Fano-like asymmetry. To rigorously confirm the underlying cause, the Raman parameters, specifically the peak position and linewidth of the TO<sub>2</sub>-TA mode, have been fitted as functions of temperature, providing quantitative insights into the mode's behaviour. These parameters are sensitive to changes in lattice dynamics, electron-phonon coupling, and electronic contributions, making them critical for distinguishing between competing mechanisms. For instance, a Fano effect typically manifests as a temperature-dependent asymmetry parameter (q) and a characteristic antiresonance dip, accompanied by an electronic background, as observed in the STO spectra<sup>9</sup>. The peak position and line width variance is plotted with the temperature range from 85 K to 300 K in fig (3.2).

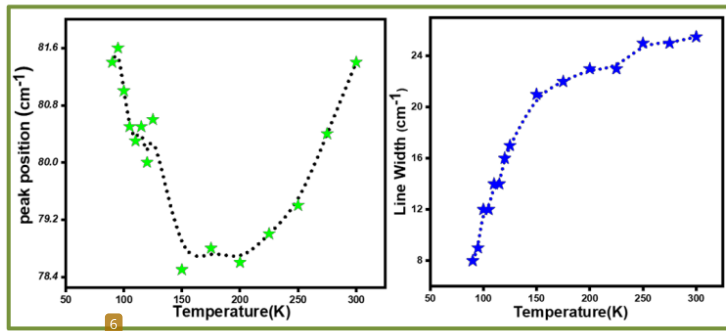


Figure 3.2: Variation in Raman peak-position with temperature for STO sample and Variation in linewidth with temperature is plotted.

4 By analysing two plots of peak position and line width as functions of temperature, distinct trends in the lattice dynamics of the material emerge. Below 150 K, the peak

position decreases with increasing temperature, indicating a reduction in phonon frequency due to intensified lattice vibrations and anharmonic coupling. Anharmonicity, the deviation from the ideal harmonic oscillator model due to non-linear terms in the potential energy, drives significant phonon interactions. These interactions cause a phonon to decay into two or three lower-energy phonons, conserving energy and momentum, which shortens the phonon lifetime and broadens the spectral line width. Concurrently, the line width increases rapidly, reflecting the decreased phonon lifetime caused by enhanced phonon decay processes. This behaviour confirms that anharmonicity dominates up to 150 K, with increased thermal energy amplifying vibrational interactions and reducing phonon frequencies. Beyond 150 K, the peak position reverses and increases with temperature, exhibiting non-linear behaviour, while the line width stabilizes, suggesting that anharmonic phonon decay is no longer the primary mechanism.

At higher temperatures, other phenomena, such as thermal expansion, electronic interactions, or higher-order scattering processes, likely become dominant, counteracting the frequency reduction and limiting further spectral broadening. There is also another statement can be said that above 150 K, in the cubic phase, the material exhibits semiconductor-like behaviour with increased charge carriers, causing the peak position to rise due to electron-phonon coupling and the line width to stabilize as scattering saturates. This transition highlights the shift from lattice-driven dynamics to charge carrier-mediated vibrational properties.

- The temperature-dependent plots of peak position and line width in strontium titanate ( $\text{SrTiO}_3$ ) show non-linear behaviour, potentially exhibiting asymmetric line shapes suggestive of the Fano effect, but it remains uncertain whether this is due to Fano resonance or other phenomena. We examined well-established publications on the Fano effect in various materials, which reveal similar non-linear trends in peak position and line width, often accompanied by asymmetric spectral features. By analyzing these materials, we seek to determine whether the observed phenomena in  $\text{SrTiO}_3$  stated from Fano resonance or other underlying mechanisms.

### 3.3 Temperature dependent Raman Spectra of heavily doped Silicon (Si) material:

A TD Raman spectroscopy have been carried out from heavily doped p-type Si<sup>14</sup> material using 532 nm laser for 520 cm<sup>-1</sup> peak to investigate the thermal response of phonons through possible phonon-phonon and electron-phonon interactions in sample.

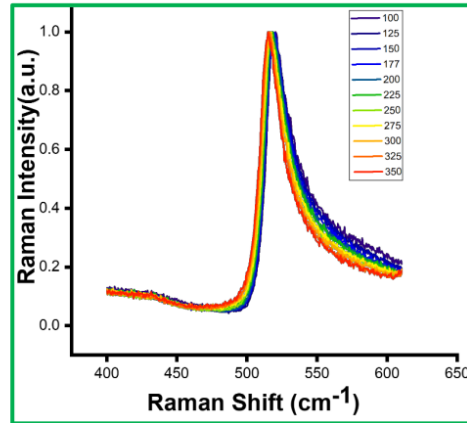


Figure 3.3 Temperature dependent Raman spectra from heavily doped p type Si using 532 nm laser for the peak at 520 cm<sup>-1</sup>.

Heavy acceptor doping significantly influences the position and width of one-phonon Raman lines in silicon (Si), as described previously. In Si, this doping leads to a "softening" of the crystal due to carrier redistribution, which shifts the phonon frequency toward lower energies in the Raman spectrum. Building on this, the temperature-dependent Raman spectrum of heavily doped Si, as shown in Figure 3.3, reveals additional complexities. As the temperature decreases, an asymmetric line shape emerges, characterized by an anti-resonance dip on the low-energy side and asymmetry on the high-energy side. This asymmetry<sup>15</sup> is supported by the Raman electron background, which indicates Fano resonance for the peak. The Fano resonance arises from the interference between the discrete phonon state and the

continuum of electronic states, further modulated by the doping-induced changes in the band structure. These observations connect directly, where doping alters the valence band and carrier dynamics, contributing to the observed spectral features and reinforcing the impact of electronic effects on the phonon behaviour in heavily doped Si.

To analyse more, how the Fano effect does vary with temperature the Raman parameter the peak position, line width and fano parameter are fitted in fig 3.4.

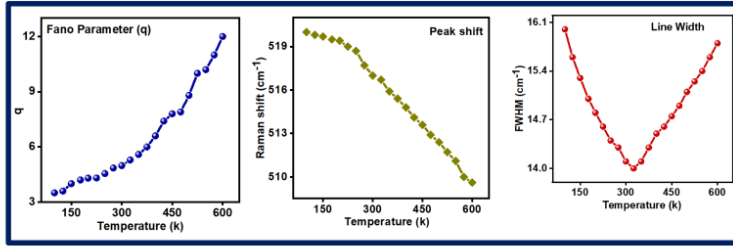


Figure 3.4: Variation in the Fano parameter, peak position and line width is plotted respectively as the temperature changes for the peak 520 cm<sup>-1</sup>.

As temperature increases, a red shift in the Raman peak position of heavily doped silicon (Si) is observed, attributed to Fano interaction, as described in Balkanski theory. This interaction arises from the quantum interference between the discrete optical phonon mode and the continuum of electronic states induced by heavy doping, as discussed earlier. The red shift reflects a decrease in phonon frequency, consistent with the “softening” of the crystal due to doping-induced carrier redistribution and valence band splitting, which lowers the crystal’s free energy. Additionally, anharmonic effects contribute to this behaviour, as evidenced by the peak shift and the reduction in line intensity with increasing temperature. Anharmonicity, stemming from nonlinear interactions between phonons, leads to thermal expansion and phonon-phonon scattering, further softening the lattice and reducing the phonon lifetime.

However, the Raman line width exhibits nonlinear behaviour with temperature. Below and up to room temperature (~300 K), the line width decreases, indicating that electron-phonon interactions dominate. These interactions, enhanced by the high



carrier concentration from heavy doping, couple the phonon to the electronic continuum, broadening the line at lower temperatures where carriers are less thermally scattered. Above room temperature, the line width increases, suggesting that anharmonic phonon-phonon interactions become dominant. This increase is driven by enhanced lattice vibrations due to thermal perturbations, which amplify phonon scattering and reduce phonon coherence.

<sup>3</sup> The Fano parameter, which quantifies the strength of the Fano resonance, increases with temperature, indicating a weakening of the Fano effect. This trend occurs because, above room temperature, anharmonic interactions overshadow the Fano interference. Thermal agitation enhances lattice vibrations, increasing the asymmetry in the Raman line shape, as observed in the temperature-dependent spectrum (Figure 3.3). This asymmetry, with an anti-resonance dip on the low-energy side and broadening on the high-energy side, aligns with the doping-induced electronic modifications discussed previously. The interplay between anharmonicity and electron-phonon coupling thus governs the Raman spectral features, with anharmonicity prevailing at higher temperatures due to increased thermal energy disrupting the delicate balance of Fano interference.

### **3.4 Temperature dependent Raman spectrum of V<sub>2</sub>O<sub>5</sub> material:**

As the previously discussed for the Silicon material the temperature dependent Raman spectrum is observed (fig 3.5) for polycrystalline V<sub>2</sub>O<sub>5</sub> material also using 532 nm laser light for the peak 995 cm<sup>-1</sup> where the Fano effect is well established in this material.

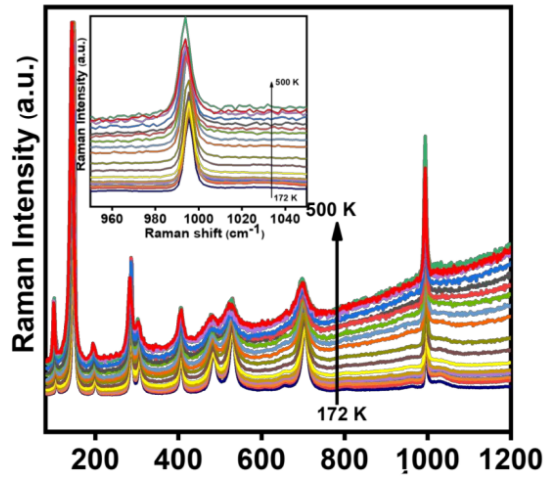


Figure 3.5: Temperature dependent Raman spectrum of  $V_2O_5$  material for the peak  $995\text{ cm}^{-1}$  and the zooming version of  $995\text{ cm}^{-1}$  (in the inset)

The temperature-dependent Raman spectrum of vanadium pentoxide ( $V_2O_5$ ) exhibits an asymmetric line shape, indicative of a Fano effect<sup>16</sup> at the  $995\text{ cm}^{-1}$  peak, associated with the  $A_g$  vibrational mode. This mode originates from the z-axis oscillation of terminal oxygen atoms, a characteristic signature of  $V_2O_5$ . The Fano effect manifests as an asymmetric spectral profile with an anti-resonance dip on the low-energy side, resulting from quantum interference between the discrete phonon<sup>17</sup> mode and a continuum of electronic states induced by photoexcitation. Excitation at  $532\text{ nm}$ , aligning with  $V_2O_5$ 's optical band gap of approximately  $2.3\text{ eV}$ , enhances resonant Raman scattering, generating charge carriers that amplify the Fano interaction. Analogous to the carrier-induced band structure modifications in heavily doped silicon, the photoexcited carriers in  $V_2O_5$  modulate phonon properties through electron-phonon coupling.

<sup>65</sup> To investigate how the asymmetry Raman line shape is varying the temperature. The peak position, line width and Fano parameter are fitted with the temperature variations in fig 3.6.

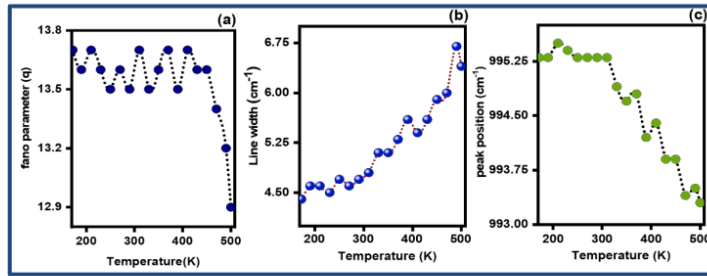


Figure 3.6 Variation in the Fano parameter, peak position<sup>56</sup> and line width is plotted respectively as the temperature changes for the peak 995 cm<sup>-1</sup>.

In the case of V<sub>2</sub>O<sub>5</sub>, the optical band gap energy<sup>7</sup> plays a crucial role in determining the resonance condition for Raman scattering. When the excitation wavelength aligns with the material's band gap energy<sup>3</sup>, it enhances the resonant Raman scattering process, leading to intensified phonon-electron interactions. This resonant condition significantly impacts the Fano parameter, as the coupling between discrete phonon modes and the continuum of electronic states becomes stronger, increasing asymmetry<sup>5</sup> in the Raman line shape. The oscillatory behaviour of the Fano parameter at lower temperatures suggests that interference effects are present but remain relatively stable, likely due to minimal fluctuations in electronic density. However, above 300 K, the rapid enhancement of the Fano strength indicates an increase in electronic interactions, potentially driven by higher thermal energy enabling more effective coupling between charge carriers and vibrational states. For linewidth broadening and peak position shifts, charge carrier dynamics and anharmonic interactions emerge as key factors. As temperature rises, carrier density<sup>18</sup> may increase, altering electron-phonon interactions and contributing to spectral modifications. Anharmonicity, arising from phonon-phonon scattering, becomes more pronounced at elevated temperatures, leading to further broadening of the Raman peaks. While phonon-phonon coupling plays a role in linewidth expansion, the charge carrier dynamics dictate peak position shifts by

modifying vibrational frequencies. The observed stability up to 300 K suggests a regime dominated by weaker phonon interactions, whereas beyond this temperature, stronger electron-phonon and anharmonic contributions drive more pronounced changes. Thus, understanding these effects allows a deeper insight into the thermal and electronic behaviour of the material, linking Raman spectral variations directly to fundamental physics concepts governing phonon and charge carrier interactions.

Beyond the 300 K threshold, pronounced changes emerge, marking a shift in the underlying scattering mechanisms. The rapid enhancement of the Fano strength, the accelerated broadening of the linewidth, and the continued decrease in peak position collectively indicate the growing influence of anharmonic interactions. At elevated temperatures, the phonon-electron coupling intensifies, amplifying the Fano effect, which becomes more dominant than anharmonicity in governing the spectral characteristics. This suggests that, as temperature increases, electronic states experience enhanced mobility or increased density, thereby strengthening their interactions with phonons. The presence of a subtle phase transition or an alteration in the electronic structure around 300 K could lead to a higher availability of continuum states, further reinforcing the Fano resonance.

These findings highlight the complexity of temperature-dependent Raman behaviour, where multiple competing effects shape the spectral response. The delicate interplay between phonon scattering, electronic interactions, and anharmonic contributions underscores the importance of detailed spectral analysis to decipher the relative contributions of each factor. The observed trends suggest that while phonon-phonon anharmonicity plays a role, it is the evolving nature of electronic states and their interaction with discrete vibrational modes that primarily govern the Raman response above 300 K. This insight provides valuable information about the underlying material properties, aiding in the interpretation of Raman spectral variations as a function of temperature. Understanding these phenomena not only contributes to fundamental condensed matter physics but also has implications for materials engineering, where controlling phonon-electron interactions can lead to the optimization of thermal and electronic properties in advanced materials systems.

### 3.5 Summary:

This chapter investigates the temperature-dependent Raman spectroscopy of heavily doped silicon (Si), vanadium pentoxide ( $\text{V}_2\text{O}_5$ ), and strontium titanate ( $\text{SrTiO}_3$ ), focusing on the interplay of phonon dynamics, electron-phonon interactions, and the Fano effect. Each material exhibits unique spectral features influenced by temperature, doping, and electronic structure, providing insights into their vibrational and electronic properties critical for applications in microelectronics, photovoltaics, and catalysis.

In heavily doped p-type silicon, the Raman spectrum of the  $520\text{ cm}^{-1}$  peak reveals a temperature-dependent Fano resonance, characterized by an asymmetric line shape with an anti-resonance dip. As temperature increases, the peak position redshifts due to lattice softening from doping-induced carrier redistribution and anharmonic phonon-phonon interactions. The linewidth decreases up to 300 K, driven by dominant electron-phonon coupling, but increases above this temperature as anharmonic effects prevail. The Fano parameter weakens with rising temperature, indicating that thermal agitation enhances anharmonicity, overshadowing Fano interference.

For polycrystalline  $\text{V}_2\text{O}_5$ , the  $995\text{ cm}^{-1}$   $\text{A}_g$  mode displays a Fano effect, marked by an asymmetric line shape due to interference between the phonon mode and photoexcited electronic states. Below 300 K, the peak position<sup>19</sup> and linewidth remain stable, with resonant Raman scattering dominating and the Fano parameter showing oscillatory but constant behaviour. Above 300 K, the Fano strength increases, the linewidth broadens rapidly, and the peak position decreases, suggesting a transition from resonant scattering to a regime where the Fano effect overshadows anharmonic interactions, possibly due to enhanced electron-phonon coupling or a subtle electronic transition.

The confirmed Fano resonance in Si and  $\text{V}_2\text{O}_5$ , characterized by temperature-dependent Fano parameter variations and asymmetric line shapes, provides a robust reference for interpreting  $\text{SrTiO}_3$ 's spectra. However, further analysis, such as fitting the Fano parameter or conducting wavelength-dependent Raman studies, is necessary to definitively confirm Fano interference in  $\text{SrTiO}_3$ . These comparative findings highlight the complex interplay of lattice dynamics, electron-phonon coupling, and quantum interference across these materials, offering valuable insights into the

vibrational properties of  $\text{SrTiO}_3$  and its potential Fano-related behaviour, with implications for its use in ferroelectric and electronic applications.

# Chapter 4

## Conclusion:

This thesis has delved into the fascinating world of perovskites, with a particular focus on strontium titanate, to uncover the intricate interplay of their structural, vibrational, and electronic properties using advanced Raman spectroscopy techniques. By exploring the phase transitions and potential Fano effects in  $\text{SrTiO}_3$ , alongside comparative studies with heavily doped silicon (Si) and vanadium pentoxide ( $\text{V}_2\text{O}_5$ ), this work has contributed to a deeper understanding of these materials' behaviors, which are pivotal for next-generation optoelectronic and energy applications. The journey through this research has been both challenging and rewarding, revealing the power of spectroscopy to probe the microscopic dynamics that govern material performance.

<sup>46</sup>  
**Chapter 2** illuminated the cubic-to-tetragonal phase transition in  $\text{SrTiO}_3$ , observed around 105 K, through polarized Raman spectroscopy. The emergence of first-order  $B_{2g}$  Raman modes at  $144\text{ cm}^{-1}$  and  $445\text{ cm}^{-1}$  at low temperatures (93 K and 88 K) confirmed the structural shift driven by soft phonon modes. The polarization-dependent intensity variations, mapped through polar plots, revealed the alignment of tetragonal domains and the material's anisotropic vibrational properties. These findings underscore  $\text{SrTiO}_3$ 's unique quantum paraelectric behavior and its sensitivity to temperature, making it a model system for studying lattice dynamics in perovskites. The consistent tetragonal symmetry across different laser wavelengths (633 nm and 532 nm) and the increasing c/a ratio at lower temperatures highlight the robustness of the phase transition, though slight misalignments in intensity maxima suggest local strains or defects that warrant further exploration.

Chapter 3 expanded the investigation to explore the potential Fano effect, a quantum interference phenomenon, in  $\text{SrTiO}_3$ , drawing comparisons with well-established Fano resonance behaviours in heavily doped Si and  $\text{V}_2\text{O}_5$ <sup>20</sup>. In heavily doped Si, the  $520\text{ cm}^{-1}$  peak exhibits clear Fano resonance, with temperature-dependent asymmetries driven by electron-phonon coupling and anharmonic interactions, as documented in prior studies. Similarly,  $\text{V}_2\text{O}_5$ 's  $995\text{ cm}^{-1}$  Ag mode shows pronounced Fano

characteristics, amplified by photoexcitation and resonant Raman scattering, particularly above 300 K, consistent with established research. In  $\text{SrTiO}_3$ , the low-frequency  $\text{TO}_2$ -TA mode displays asymmetric line shapes that suggest possible Fano interference, but definitive confirmation remains elusive due to competing mechanisms, such as anharmonic phonon interactions. By leveraging the known nonlinear behaviours of Si and  $\text{V}_2\text{O}_5$  as a reference<sup>21</sup>, this study proposes a framework for investigating potential Fano effects in complex oxides like  $\text{SrTiO}_3$ , providing insights into its enigmatic low-temperature behaviour and its prospects in oxide electronics.

The significance of this work lies not only in its scientific contributions but also in its implications for real-world applications. Perovskites like  $\text{SrTiO}_3$  are at the forefront of sustainable energy technologies, from high-efficiency solar cells to tunable electronic devices. Understanding their phase transitions and electron-phonon interactions is crucial for optimizing their performance in harsh conditions, such as varying temperatures. The methodologies developed here, particularly the use of temperature-dependent and polarized Raman spectroscopy, provide a blueprint for studying other perovskite materials, paving the way for innovations in microelectronics, photovoltaics, and catalysis.



## REFERENCES

1. Assirey, E. A. R. Perovskite synthesis, properties and their related biochemical and industrial application. *Saudi Pharmaceutical Journal* **27**, 817–829 (2019).
2. Magnetic, Electronic, and Optical Properties of Perovskite Materials | SpringerLink. [https://link.springer.com/chapter/10.1007/978-981-15-1267-4\\_2](https://link.springer.com/chapter/10.1007/978-981-15-1267-4_2).
3. Figure 1. Schematic illustration of the perovskite crystal structure... *ResearchGate* [https://www.researchgate.net/figure/Schematic-illustration-of-the-perovskite-crystal-structure-where-A-and-B-are-cations-and\\_fig1\\_361880950](https://www.researchgate.net/figure/Schematic-illustration-of-the-perovskite-crystal-structure-where-A-and-B-are-cations-and_fig1_361880950).
4. Saito, R., Tatsumi, Y., Huang, S., Ling, X. & Dresselhaus, M. S. Raman spectroscopy of transition metal dichalcogenides. *J. Phys.: Condens. Matter* **28**, 353002 (2016).
5. Full article: Polarized Raman Spectra of BaTiO<sub>3</sub>/SrTiO<sub>3</sub> Superlattices. <https://www.tandfonline.com/doi/full/10.1080/00150190500314833>.
6. TN199EN\_01\_A\_Polarised\_Raman\_spectroscopy\_using\_the\_inVia\_Raman\_microscope.pdf.
7. Rani, C. *et al.* Non-linear temperature dependent Raman parametric changes: An identification of Fano intervened systems. *Physics Reports* **1037**, 1–41 (2023).
8. Enhanced dielectric properties of barium strontium titanate thin films by doping modification | Journal of Materials Science: Materials in Electronics. <https://link.springer.com/article/10.1007/s10854-019-01670-w>.

9. Nilsen, W. G. & Skinner, J. G. Raman Spectrum of Strontium Titanate. *The Journal of Chemical Physics* **48**, 2240–2248 (1968).
10. Gray, D. J., Merz, T. A., Hikita, Y., Hwang, H. Y. & Mabuchi, H. Orientation-resolved domain mapping in tetragonal  $\text{SrTiO}_3$  using polarized Raman spectroscopy. *Phys. Rev. B* **94**, 214107 (2016).
11. Sirenko, A. A. *et al.* Observation of the First-Order Raman Scattering in  $\text{SrTiO}_3$  Thin Films. *Phys. Rev. Lett.* **82**, 4500–4503 (1999).
12. Chapman, P. W., Tufte, O. N., Zook, J. D. & Long, D. Electrical Properties of Heavily Doped Silicon. *Journal of Applied Physics* **34**, 3291–3295 (1963).
13. Balachandran, U. & Eror, N. G. Raman Spectra of Strontium Titanate. *Journal of the American Ceramic Society* **65**, c54–c56 (1982).
14. K. Saxena, S. *et al.* Amplification or cancellation of Fano resonance and quantum confinement induced asymmetries in Raman line-shapes. *Physical Chemistry Chemical Physics* **19**, 31788–31795 (2017).
15. Qualitative Evolution of Asymmetric Raman Line-Shape for NanoStructures I Silicon. <https://link.springer.com/article/10.1007/s12633-013-9176-9>.
16. Rath, D. K. *et al.* Resonant Electron–Phonon Interaction and Its Non-Fano-Type Wavelength and Power-Dependent Raman Manifestation. *J. Phys. Chem. C* **128**, 15186–15193 (2024).
17. Lineshape analysis of Raman scattering from LO and SO phonons in III-V nanowires | Journal of Applied Physics | AIP Publishing.

<https://pubs.aip.org/aip/jap/article/106/11/114317/900394/Lineshape-analysis-of-Raman-scattering-from-LO-and>.

18. M, N. K. *et al.* Size Dependent Sensitivity of Raman Line-Shape Parameters in Silicon Quantum Wire. *Advances in Materials and Processing Technologies* **6**, 669–676 (2020).
19. Kumar Rath, D. *et al.* Nonlinear Fano-Raman line-shape evolution: direct evidence of the creation and annihilation of interferons in V<sub>2</sub>O<sub>5</sub>. *Physical Chemistry Chemical Physics* **27**, 8674–8679 (2025).
20. Resonant Fano interaction in B1g/B3g Raman mode under off-resonant excitation in V<sub>2</sub>O<sub>5</sub>  $\mu$ -crystals: Thermal phonon as facilitator: iScience. [https://www.cell.com/iscience/fulltext/S2589-0042\(25\)00397-9](https://www.cell.com/iscience/fulltext/S2589-0042(25)00397-9).
21. Blue- and red-shifts of V<sub>2</sub>O<sub>5</sub> phonons in NH<sub>3</sub> environment by in situ Raman spectroscopy - IOPscience. <https://iopscience.iop.org/article/10.1088/1361-6463/aa98fe/meta>.

## ORIGINALITY REPORT

14%

SIMILARITY INDEX

7%

INTERNET SOURCES

11%

PUBLICATIONS

3%

STUDENT PAPERS

## PRIMARY SOURCES

1

[dspace.iiti.ac.in:8080](https://dspace.iiti.ac.in:8080)

Internet Source

2%

2

[link.aps.org](https://link.aps.org)

Internet Source

1%

3

Deb Kumar Rath, Shivansh Raj Pandey, Abhishek S. Shekhawat, Love Bansal et al. "Resonant Fano interaction in B1g/B3g Raman mode under Off-Resonant Excitation in V2O5  $\mu$ -crystals: Thermal phonon as facilitator", iScience, 2025

Publication

1%

4

Chanchal Rani, Manushree Tanwar, Suchita Kandpal, Tanushree Ghosh, Love Bansal, Rajesh Kumar. "Nonlinear Temperature-Dependent Phonon Decay in Heavily Doped Silicon: Predominant Interferon-Mediated Cold Phonon Annihilation", The Journal of Physical Chemistry Letters, 2022

Publication

1%

5

Nourhan Barakat, Fouad El Haj Hassan, Michel Kazan. "Modulating phonon-electron Fano resonance in Si nanoparticles through laser exposure and properties of surrounding nanoparticles", Journal of Physics and Chemistry of Solids, 2025

Publication

<1%

6

C Rani, S Kandpal, T Ghosh, Love Bansal, Manushree Tanwar, Rajesh Kumar. "Energy Dispersive Anti-anharmonic Effect in Fano

<1%

Intervened Semiconductor: Revealing through temperature and wavelength dependent Raman scattering", Physical Chemistry Chemical Physics, 2022

Publication

---

7 "Raman Spectroscopy", Springer Science and Business Media LLC, 2024 <1 %

Publication

---

8 Submitted to Indian Institute of Management, Indore <1 %

Student Paper

---

9 R. Gupta, Q. Xiong, C. K. Adu, U. J. Kim, P. C. Eklund. "Laser-Induced Fano Resonance Scattering in Silicon Nanowires", Nano Letters, 2003 <1 %

Publication

---

10 Fernando Cerdeira, T. A. Fjeldly, M. Cardona. " Effect of Free Carriers on Zone-Center Vibrational Modes in Heavily Doped -type Si. II. Optical Modes ", Physical Review B, 1973 <1 %

Publication

---

11 Deb Kumar Rath, Love Bansal, Kuldeep Barwa, Bhumika Sahu, Nikita Ahlawat, Subin Kaladi Chondath, Rajesh Kumar. " Nonlinear Fano-Raman line-shape evolution: direct evidence of the creation and annihilation of interferons in V O ", Physical Chemistry Chemical Physics, 2025 <1 %

Publication

---

12 Submitted to University of Surrey <1 %

Student Paper

---

13 [www.science.gov](http://www.science.gov) <1 %

Internet Source

---

14 Chanchal Rani, Manushree Tanwar, Tanushree Ghosh, Suchita Kandpal, <1 %

Shailendra K. Saxena, Rajesh Kumar. "Non-linear temperature dependent Raman parametric changes: An identification of Fano intervened systems", Physics Reports, 2023

Publication

- 
- |           |   |      |
|-----------|---|------|
| <b>15</b> | Submitted to University College Dublin (UCD)<br>Student Paper | <1 % |
|-----------|---|------|
- 
- |           |   |      |
|-----------|---|------|
| <b>16</b> | <a href="http://libjncir.jncasr.ac.in">libjncir.jncasr.ac.in</a><br>Internet Source | <1 % |
|-----------|---|------|
- 
- |           |   |      |
|-----------|---|------|
| <b>17</b> | <a href="http://www.nature.com">www.nature.com</a><br>Internet Source | <1 % |
|-----------|---|------|
- 
- |           |  |      |
|-----------|--|------|
| <b>18</b> | Ferroelectric Materials and Ferroelectricity, 1970.<br>Publication | <1 % |
|-----------|--|------|
- 
- |           |  |      |
|-----------|--|------|
| <b>19</b> | Gray, Dodd Joseph, Jr.. "Crystal Domain Mapping with Polarized Raman Spectroscopy and Chi-(2) Nonlinear Optics in CMOS Waveguides", Stanford University, 2020<br>Publication | <1 % |
|-----------|--|------|
- 
- |           |   |      |
|-----------|---|------|
| <b>20</b> | Jingxian Xiong, Zhiying Dan, Hengyi Li, Sina Li, Yiming Sun, Wei Gao, Nengjie Huo, Jingbo Li. "Multifunctional GeAs/WS Heterojunctions for Highly Polarization-Sensitive Photodetectors in the Short-Wave Infrared Range ", ACS Applied Materials & Interfaces, 2022<br>Publication | <1 % |
|-----------|---|------|
- 
- |           |  |      |
|-----------|--|------|
| <b>21</b> | Li, Shuang Bin, Ying Yao, Yong Zhong Jia, Jing Yan, and Shao Lei Xie. "Raman Spectra of SrTiO <sub>3</sub> Prepared by Direct Current Arc Discharge Plasma Process", Advanced Materials Research, 2014.<br>Publication | <1 % |
|-----------|--|------|
- 
- |           |   |      |
|-----------|---|------|
| <b>22</b> | <a href="http://www.mdpi.com">www.mdpi.com</a><br>Internet Source | <1 % |
|-----------|---|------|
-

23 Alexander Tkach. "Antiferrodistortive phase transition in doped strontium titanate ceramics: The role of the perovskite lattice vacancies", Elsevier BV, 2023 <1 %

---

Publication

24 Azza Hadj Youssef, Jiawei Zhang, Alborz Ehteshami, Gitanjali Kolhatkar et al. "Symmetry-Forbidden-Mode Detection in SrTiO Nanolands with Tip-Enhanced Raman Spectroscopy ", The Journal of Physical Chemistry C, 2021 <1 %

---

Publication

25 Stuart J. Henderson, Olga Shebanova, Andrew L. Hector, Paul F. McMillan, Mark T. Weller. " Structural Variations in Pyrochlore-Structured Bi Hf O , Bi Ti O and Bi Hf Ti O Solid Solutions as a Function of Composition and Temperature by Neutron and X-ray Diffraction and Raman Spectroscopy ", Chemistry of Materials, 2007 <1 %

---

Publication

26 Submitted to University of Lincoln <1 %

---

Student Paper

27 Liangbo Liang, Jun Zhang, Bobby G. Sumpter, Qing-Hai Tan, Ping-Heng Tan, Vincent Meunier. "Low-Frequency Shear and Layer-Breathing Modes in Raman Scattering of Two-Dimensional Materials", ACS Nano, 2017 <1 %

---

Publication

28 Submitted to Amrita Vishwa Vidyapeetham <1 %

---

Student Paper

29 Kaushal, Ken. "Pushing the Bounds of Halide Perovskite Solar Cell Stability Using a Streamlined, Automated Platform for <1 %

Fabrication and Testing", University of  
California, San Diego, 2024

Publication

- 30 Fen Zhang, Yali Yu, Zhangxun Mo, Le Huang, Qinglin Xia, Bo Li, Mianzeng Zhong, Jun He. "Alloying-engineered high-performance broadband polarized Bi<sub>1.3</sub>In<sub>0.7</sub>Se<sub>3</sub> photodetector with ultrafast response", Nano Research, 2022

Publication

- 31 Submitted to Indian Institute of Technology <1 %

Student Paper

- 32 Y.D. Juang, S.B. Dai, Y.C. Wang, W.Y. Chou, J.S. Hwang, M.L. Hu, W.S. Tse. "Phase transition of Li<sub>x</sub>Na<sub>1-x</sub>NbO<sub>3</sub> studied by Raman scattering method", Solid State Communications, 1999

Publication

- 33 [arch.library.northwestern.edu](http://arch.library.northwestern.edu) <1 %

Internet Source

- 34 Jayasree, R.S.. "Temperature dependent polarized Raman spectra of nonaqua lanthanoid (Pr) single crystal", Spectrochimica Acta Part A: Molecular and Biomolecular Spectroscopy, 20060515

Publication

- 35 [mafiadoc.com](http://mafiadoc.com) <1 %

Internet Source

- 36 [www.ebi.ac.uk](http://www.ebi.ac.uk) <1 %

Internet Source

- 37 [www.mrs.org](http://www.mrs.org) <1 %

Internet Source

- 38 Alen Sam Thomas, Philip Nathaniel Immanuel, Neena Prasad, Achiad Goldreich, Jonathan Prilusky, Raanan Carmieli, Lena Yadgarov. "



Synthesis of CsPbBr decorated ZIF-8  
nanocomposite for enhanced photocatalytic  
performance ", Nanoscale Advances, 2025

Publication

39

Eric McCalla, Jeff Walter, Chris Leighton. " A  
Unified View of the Substitution-Dependent  
Antiferrodistortive Phase Transition in SrTiO ",  
Chemistry of Materials, 2016

<1 %

Publication

40

Luders, M.. "Impurity-lattice coupling in  
SrTiO<sup>3</sup>: Eu<sup>3+</sup>", Solid State  
Communications, 19690415

<1 %

Publication

41

[smartech.gatech.edu](http://smartech.gatech.edu)

Internet Source

<1 %

42

[www.researchgate.net](http://www.researchgate.net)

Internet Source

<1 %

43

"Materials for Electronic, Magnetic, and  
Spintronic Technologies", Springer Science  
and Business Media LLC, 2024

<1 %

Publication

44

Chanchal Rani, Deb Kumar Rath, Anjali  
Ghanghass, Tanushree Ghosh et al. " Quasi-  
Fano Resonance-Induced Asymmetric Raman  
Mode in WS Nanoflakes ", The Journal of  
Physical Chemistry C, 2023

<1 %

Publication

45

D. M. Sagar, Joanna M. Atkin, Peter K. B.  
Palomaki, Nathan R. Neale et al. "Quantum  
Confined Electron–Phonon Interaction in  
Silicon Nanocrystals", Nano Letters, 2015

<1 %

Publication

46

S. Klauer. "Incorporation of hydrogen in cubic  
and uniaxial oxidic crystals deduced from

<1 %

47

Shailendra K. Saxena, Priyanka Yogi,  
Suryakant Mishra, Hari Mohan Rai et al.

"Amplification or cancellation of Fano  
resonance and quantum confinement  
induced asymmetries in Raman line-shapes",  
Physical Chemistry Chemical Physics, 2017

Publication

<1 %

48

[docksci.com](https://docksci.com)

Internet Source

<1 %

49

[pdfs.semanticscholar.org](https://pdfs.semanticscholar.org)

Internet Source

<1 %

50

Federico A. Rabuffetti, Peter C. Stair, Kenneth  
R. Poeppelmeier. " Synthesis-Dependent  
Surface Acidity and Structure of SrTiO  
Nanoparticles ", The Journal of Physical  
Chemistry C, 2010

Publication

<1 %

51

Lin, Jing-Jing, Li-Wei Guo, Yu-Ping Jia, Lian-Lian  
Chen, Wei Lu, Jiao Huang, and Xiao-Long  
Chen. "Effect of 6H-SiC (112?0) substrate on  
epitaxial graphene revealed by Raman  
scattering", Chinese Physics B, 2013.

Publication

<1 %

52

Shengxi Huang, Yuki Tatsumi, Xi Ling,  
Huaihong Guo et al. "In-Plane Optical  
Anisotropy of Layered Gallium Telluride", ACS  
Nano, 2016

Publication

<1 %

53

Suk Bong Hong. "Vibrational spectroscopic  
evidence for the presence of TiO<sub>6</sub> structural  
units in titanosilicate molecular sieve ETS-10",

<1 %

---

54	dais.sanu.ac.rs	<1 %
	Internet Source	

---

55	iopscience.iop.org	<1 %
	Internet Source	

---

56	roderic.uv.es	<1 %
	Internet Source	

---

57	vsip.info	<1 %
	Internet Source	

---

58	www.db-thueringen.de	<1 %
	Internet Source	

---

59	www.nanotechmag.com	<1 %
	Internet Source	

---

60	Manushree Tanwar, Anjali Chaudhary, Devesh K. Pathak, Priyanka Yogi, Shailendra K. Saxena, Pankaj R. Sagdeo, Rajesh Kumar. "Deconvoluting Diffuse Reflectance Spectra for Retrieving Nanostructures' Size Details: An Easy and Efficient Approach", The Journal of Physical Chemistry A, 2019	<1 %
	Publication	

---

61	Manushree Tanwar, Devesh K. Pathak, Chanchal Rani, Suchita Kandpal et al. "Inverse Size Dependent Fano Parameter in Silicon Porous Wires: Consequence of Quasi-Continuum Flattening", The Journal of Physical Chemistry C, 2021	<1 %
	Publication	

---

62	S. A. Hayward. "Cubic-tetragonal phase transition in SrTiO <sub>3</sub> revisited: Landau theory and transition mechanism", Phase Transitions, 4/1/1999	<1 %
	Publication	

---

63 Veera Krasnenko, Leonid L. Rusevich, Aleksander Platonenko, Yuri A. Mastrikov, Maksim Sokolov, Eugene A. Kotomin. "Water Splitting on Multifaceted SrTiO<sub>3</sub> Nanocrystals: Calculations of Raman Vibrational Spectrum", Materials, 2022

<1 %

Publication

---

64 Federico A. Rabuffetti, Hack-Sung Kim, James A. Enterkin, Yingmin Wang et al. " Synthesis-Dependent First-Order Raman Scattering in SrTiO Nanocubes at Room Temperature ", Chemistry of Materials, 2008

<1 %

Publication

---

65 Minal Gupta, Anil Kumar, Archana Sagdeo, Pankaj R. Sagdeo. " Doping-Induced Combined Fano and Phonon Confinement Effect in La-Doped CeO : Raman Spectroscopy Analysis ", The Journal of Physical Chemistry C, 2021

<1 %

Publication

---

66 Roberto L. Moreira, Ricardo P. S. M. Lobo, Ganesanpotti Subodh, Mailadil T. Sebastian, Franklin M. Matinaga, Anderson Dias. " Optical Phonon Modes and Dielectric Behavior of Sr Ce TiO Microwave Ceramics ", Chemistry of Materials, 2007

<1 %

Publication

---